THESIS FOR THE DEGREE OF LICENTIATE OF ENGINEERING

# The Formation of White Layers and its Impact on Surface Integrity of Hard-Turned Tempered Martensitic Bearing Steels

SAHITH KOKKIRALA


CHALMERS

Department of Industrial and Materials Science
CHALMERS UNIVERSITY OF TECHNOLOGY
Gothenburg, Sweden, 2024

**The Formation of White Layers and its Impact on Surface Integrity of Hard-Turned Tempered Martensitic Bearing Steels**

SAHITH KOKKIRALA



Technical report no IMS-2024-8

Licentiate Thesis at Chalmers University of Technology

Department of Industrial and Materials Science

Chalmers University of Technology

SE-412 96 Gothenburg

Sweden

Tel: +46 (0)31 772 1000

Printed by Chalmers Reproservice

Gothenburg, Sweden 2024

*To my father Sanjeeva Rao K, mother Srilatha K, and brother Rohith K*

# The Formation of White Layers and its Impact on Surface Integrity of Hard-Turned Tempered Martensitic Bearing Steels

SAHITH KOKKIRALA
Department of Industrial and Materials Science
Chalmers University of Technology

**Abstract**

With the rapid advancement of manufacturing methods, machined components are expected to exhibit improved surface integrity and enhanced functional performance. To achieve better surface integrity and dimensional precision, traditionally hardened steels (> 45 HRC) often undergo grinding and polishing operations. With the recent advancement in the machining process and the progress of new cutting tool materials, high precision, and better surface integrity can be obtained by hard turning process with shorter resetting time using PCBN inserts. However, depending on the cutting conditions, the interaction between the workpiece and cutting tool induces gradients of thermo-mechanical loads on the machined surface resulting in white layer formation.

To understand the white layer formation and its characteristics, the first part of this thesis investigates the effects of cutting parameters and tool geometry on the formation of white layers and their impact on the surface integrity of hard-turned AISI 52100 bearing steel. The results revealed distinctive microstructural morphology in the white layers generated by dominant mechanical and thermal loads, i.e. mechanically induced white layer (M-WL) and thermally induced white layer (T-WL). The M-WL exhibited an elongated, fragmented microstructure with a material drag zone underneath it. M-WL showed ~26% increased hardness, while the material drag showed ~6% increased hardness compared to the bulk material. Additionally, better surface roughness and higher surface compressive residual stresses were observed. In contrast to M-WL, the T-WL exhibited a cellular structure with a dark layer adjacent to it. Under thermal dominant conditions, there was an increase in surface roughness and reduced surface compressive stresses with fresh inserts compared to M-WL, and even observed surface tensile stresses with worn inserts. The T-WL exhibited ~28% higher hardness, while the dark layer beneath resulted in 17% lower hardness than the bulk material.

The second part of the thesis investigates the role of varying retained austenite (RA) content in the white layer formation. The results showed that, regardless of the RA content, M-WLs associated with surface compressive residual stresses were observed at low cutting speed using fresh cutting inserts. With a worn tool, samples with higher RA content resulted in the formation of T-WL which was accompanied by surface tensile residual stresses. A similar observation was made when machining at high cutting speed using a fresh cutting insert. Regardless of RA content, machining at high cutting speed with a worn cutting tool, led to T-WL at the surface, which was accompanied by surface tensile residual stresses.

This work shows the effect of cutting conditions and different retained austenite content on the formation of M-WL and T-WL in AISI 52100 bearing steel. The results highlight the improved surface integrity capability of the M-WL compared to T-WL.

**Keywords:** hard-turning, martensite, AISI 52100, white layer, dark layer, surface roughness, residual stresses, retained austenite, nanoindentation

# Preface

This licentiate thesis is based on the work performed in the Department of Industrial and Materials Science at Chalmers University of Technology from October 2021 to May 2024. The work was carried out under the supervision of Professor Uta Klement and Dr Seyed B. Hosseini (RISE AB) as part of the project "*Flexible and sustainable production of high-performance rolling bearings*" (Turn2Flex) funded by the Swedish Governmental Agency for Innovation Systems (VINNOVA).

The thesis consists of two sections: a summary of the performed work and the appended papers.

List of appended papers:

**PAPER A** **Effect of cutting parameters on the generated surface integrity of hard-turned martensitic AISI 52100 bearing steel**
Sahith Kokkirala, Jonas Holmberg, Uta Klement, Roger Lundstrom, Hirotsugu Iwasaki, Seyed B Hosseini
*Procedia CIRP, Volume 115, 10th CIRP Global Web Conference – Material Aspects of Manufacturing Processes, 2022, Pages 154-159*
https://doi.org/10.1016/j.procir.2022.10.066

**PAPER B** **Characterization of Mechanically and Thermally Induced White Layers Formed during Hard Turning of AISI 52100 Steel**
Sahith Kokkirala, Uta Klement, Jonas Holmberg, Juan M B Bermejo, Stefan Kimming, Hirotsugu Iwasaki, Seyed B. Hosseini
*Manuscript*

**PAPER C** **The role of retained austenite on the formation of the nanostructured hard-turned induced white layer in AISI 52100 bearing steel**
S. Kokkirala, K. Osman, J. Holmberg, S. Kimming, H. Iwasaki, U. Klement, S.B. Hosseini
*Manuscript accepted by Procedia CIRP, 7th CIRP Conference on Surface Integrity, 2024.*

**Contribution to the appended papers:**

**PAPER A:** The work was planned in collaboration with supervisors. The author carried out the experimental work, except for the hard-turning tests that were performed at Sumitomo and the surface roughness measurements carried out by Dr. Jonas Holmberg at RISE AB. The author analyzed the data and wrote the paper in collaboration with the co-authors.

**PAPER B:** The work was planned in collaboration with the supervisors. The author performed the experimental work, except for the hard-turning tests that were performed at Sumitomo and surface roughness measurements carried out by Dr. Jonas Holmberg (RISE AB). Nanoindentation experiments were performed at Micro Materials Ltd, but the initial tests were performed by Juan Manuel Bello Bermejo (Lund University) and by the author to determine the test parameters. The author analyzed the data and wrote the paper in collaboration with the co-authors.

**PAPER C:** The work was planned in collaboration with supervisors and was executed by Karim Osman as his MSc thesis work under the author's supervision. The hard-turning tests were carried out at SKF. The SEM analysis was performed by the author. The author analyzed the data and wrote the paper in collaboration with the co-authors.

# Contents

# CHAPTER 1

# Introduction

## 1.1 Motivation

High-quality steel products with superior dimensional precision and surface integrity are required for various functional performances. Often machining is performed as a final finishing operation to achieve the product requirements manufactured by forging, casting, rolling and various other shaping processes. The machining of hardened steel components is receiving significant attention due to its numerous applications in industries such as automotive, press tooling, die molding, gear manufacturing, bearing applications, and aeronautics. Traditionally, the grinding process is performed followed by honing as a final finishing process for the hardened steels. However, in recent years, there has been a growing acceptance of hard-turning as a competitive alternative to grinding. This is due to its ability to achieve required surface integrity specifications, higher flexibility in the manufacturing process, lower energy consumption, high material removal rate, and manufacturing of complex geometries using Polycrystalline Cubic Boron Nitride (PCBN) cutting inserts [1], [2], [3].

During the hard-turning process, the workpiece material experiences high strain rates from thermo-mechanical loads, which often leads to the generation of a thin layer on the machined surface referred to as the 'white layer'. The thin layer appears featureless when viewed under optical microscopy [4], [5], [6], [7]. Consequently, the machined component exhibits different surface and subsurface alterations in terms of

microstructure compared to the bulk material, thereby compromising its surface integrity.

Depending on the cutting conditions during the hard-turning process, mechanically-induced and thermally-induced white layers are generated. The white layer consists of nanocrystalline grains and ultra-fine grains (20 nm to 200 nm) and possesses higher hardness than the bulk material [8], [9], [10]. Due to the anticipated enhanced wear resistance and hardness properties at the surface, tailoring the formation mechanism of nanocrystalline microstructure with required surface roughness and compressive residual stresses might increase the functional performances of the engineered component through hard-turning. However, the practical limitations of the white layer performances are uncertain depending on the formation mechanism. To address this research gap, this thesis aims to investigate the characteristics of hard-turned induced white layers to potentially be used as functional surfaces.

## 1.2 Research objective

The main aim of this research project is to understand the surface integrity generated by the hard-turning process on AISI 52100 through hardened bearing steel with a tempered martensitic microstructure. The interaction between the workpiece material and the cutting tool during the hard-turning process creates gradients of thermo-mechanical loads such as stress, temperature, and plastic deformation on the machined surface, leading to the formation of the white layer.

Depending on the cutting conditions, the mechanism behind the formation of white layers on the machined surface, along with their corresponding surface integrity and mechanical properties, is unlikely to be similar. This study aims to investigate the surface integrity and mechanical properties of the white layers generated by mechanical and thermal dominance with various cutting conditions.

This project is designed to investigate the following research questions related to the hard-turning of AISI 52100 bearing steel:

- *Q1: What is the effect of cutting parameters and cutting tool geometry on the surface integrity of the hard-turned AISI 52100 steel?*

- *Q2: What is the role of retained austenite in the formation of hard-turned induced white layers?*

## 1.3 Research outline

Chapter 2 provides a comprehensive understanding of the background of machining-induced white layers and then hard-turned induced white layers. To understand the formation mechanism of mechanically-induced white layers and thermally-induced white layers, the concept of dynamic recovery and dynamic recrystallization is discussed. The purpose of this review is to offer the reader valuable background information regarding the initial studies of white layers formed by machining.

Chapter 3 explains the chemical composition of the material, heat treatments, and initial microstructure before hard-turning machining. Additionally, it explains the heat treatment process generating different fractions of retained austenite.

Chapter 4 introduces the theory of hard turning. In addition, the surface integrity resulting from the hard turning process is discussed in terms of residual stresses and surface roughness. The focus is particularly on the effect of various cutting parameters and the progression of tool flank wear.

Chapter 5 outlines the experimental details and process conditions connected to the different characterization techniques used to study the white layers. The residual stresses are evaluated with X-ray diffraction (XRD), surface roughness is studied with an optical profilometer using coherence scanning interferometry technique, the microstructural investigation is performed with light optical microscopy (LOM), scanning electron microscopy (SEM), and finally, nanoindentation to understand the mechanical properties.

Chapter 6 summarizes the obtained results in connection to the research questions discussing the effect of cutting parameters on white layer formation, the characteristics of white layers, and the role of retained austenite in the formation of white layers.

Chapter 7 provides the conclusions and insights into the future scope of the work.

# CHAPTER 2

# White Layers

## 2.1 Background

"White layer" refers to the microstructural alteration of the bulk metallic material and due to their etch-resistant behaviour, they appear featureless and white when viewed under the light optical microscope. They are usually observed in a range of ferrous and non-ferrous materials under different conditions. In 1912, Stead was the first to observe the presence of white layers on steel wire ropes after use [11]. He determined that these white layers are formed because of frictional heating, followed by rapid cooling (quenching), which occurred during service. The occurrence of white layers has been reported in machining operations like hard-turning [8], [9], grinding [7], milling [12], drilling [13], reaming [14], and electrical discharge machining [6], [15]. Apart from machining, additionally, they are observed during rail-wheel interactions [16] and impact loading testing [10].

The appearance of the white layer on the sample cross-section when observed under a light optical microscope (LOM) is due to the scattering of the white light when the surface interacts with the visible light. The fine features in the altered region are smaller than the visible wavelength of light (400 nm – 700 nm) contributing to this white light scattering. However, when the white layer is examined using a scanning electron microscope (SEM), the higher resolution capability of the SEM allows for the visualization of very fine features within the white layer region. Figure 1 shows the hard-turned induced white layer observed in LOM and SEM.

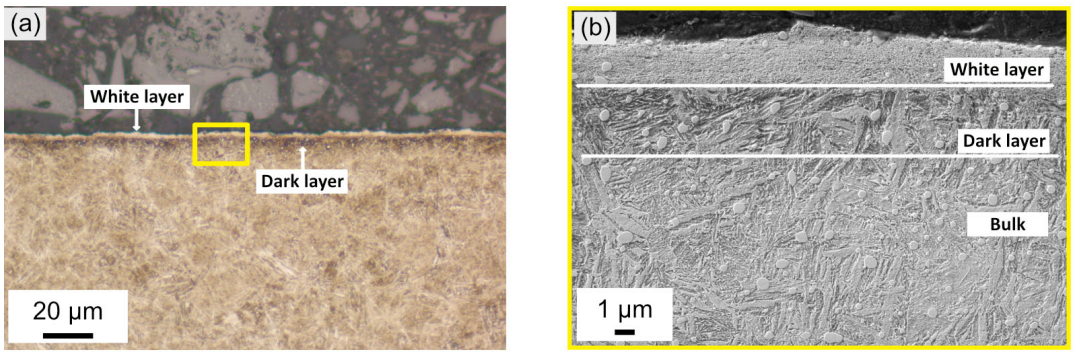


*Figure 1: White layer microstructure in AISI 52100 tempered martensite bearing steel machined by hard-turning observed by (a) light optical microscopy and (b) scanning electron microscope.*

The white layer is often observed with a subsurface microstructural transformation known as the 'dark layer'. The generated white and dark layers on the machined surface exhibit different microstructural properties compared to the bulk material. The microstructure of the white layer is usually characterized by untempered martensite formed via reverse martensitic transformation. Conversely, the dark layer is composed of over-tempered martensite [17], [18]. However, because of various process conditions, the generated white layer might not observe a dark layer beneath it. When Turley [14] investigated the white etching surfaces formed during the reaming process in ultra-high-strength steel, he concluded that the white layer with a fine subgrain structure is formed due to surface fragmentation that occurs from severe plastic deformation. There is no occurrence of dark layers beneath it, but a plastic deformation layer as observed in Figure 2 (a). Figure 2 (b) shows the mechanically induced white layers generated by the hard turning process with no dark layer beneath in AISI 52100 tempered martensitic bearing steel.

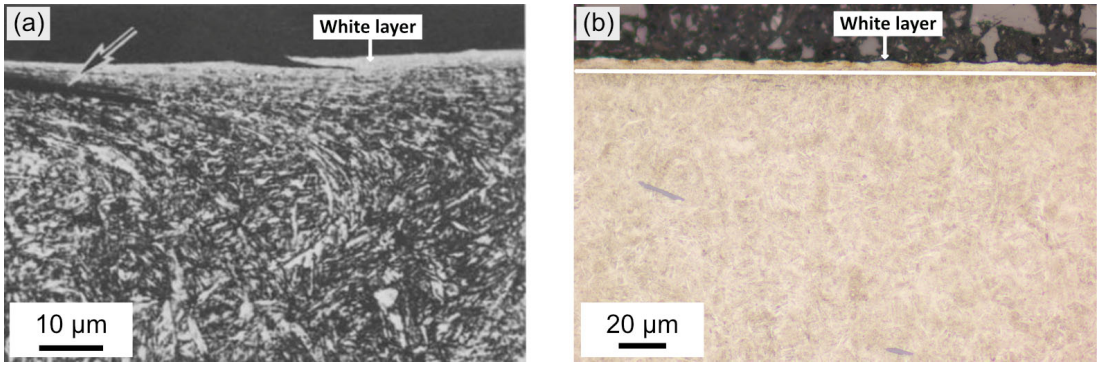


*Figure 2: (a) White etching surface formed by the reaming process with a plastic deformation layer beneath it. The arrow indicates a defect. Taken with permission from Ref.* [14]. *(b) Mechanically-induced white layer generated by the hard-turning process with no dark layer beneath it in AISI 52100 tempered martensitic bearing steel.*

Numerous researchers have investigated the formation of white layers, with Griffiths [4] suggesting three mechanisms leading to their generation: (a) the development of a very fine grain structure due to severe plastic deformation

(mechanical effect), (b) phase transformation resulting from rapid heating and quenching (thermal effect), and (c) surface reaction triggered by environmental factors. However, when machining the hardened steels, the focus is primarily on the mechanical and thermal effects in the formation of white layers.

## 2.2 Hard-turned induced white layers

The hard turning process refers to the machining of metallic materials with a hardness exceeding 45 HRC. During this process, the machined surface undergoes simultaneous mechanical and thermal effects. The formation of the white layer during the hard-turning process was examined in 1976 by Bailey et al. [19]. He observed the white layers on the hardened AISI 4340 steel when machined using a tungsten carbide cutting tool with varying cutting speeds and artificially generated controlled wear land. He concluded that under high cutting speeds and extensive tool wear, the observed white layers are the result of a phase transformation due to the elevated temperatures generated by the tool and the workpiece interaction.

Chou and Evans [17] studied the white layer formation on hard-turned AISI 52100 steel using a worn $Al_2O_3$-TiC ceramic tool. As the cutting speed increased, the thickness of the white layer increased, but after a certain speed, the rate of increase gradually decreased. However, with the increase of tool wear, the white layer thickness increased progressively. The XRD results from the study showed an increased retained austenite content of 33% in the white layer in comparison to 11% in the bulk material. The high retained austenite content in the white layer was concluded to be due to thermally driven reverse martensitic transformation with possible activation of plastic strain.

Cutting speed and tool wear are the primary interests in the hard-turning process because of their intricate influence on thermo-plastic deformation. Several researchers have made similar observations about high retained austenite content and the formation of a dark layer beneath the white layer, and that the white layer formed during hard turning is influenced by increasing cutting speed and tool wear interactions [9], [20], [21], [22].

In the literature, it is often assumed that the white layer forms when the surface temperature of the workpiece surpasses the austenitization temperature in the equilibrium Fe-C phase diagram due to the reverse martensitic phase transformation effect ($\gamma \rightarrow \alpha$). The fine grain structure in the white layer region is formed due to dynamic recovery followed by the dynamic recrystallization process. Zhang et al. [21] investigated the formation of the dark layer beneath white layers in AISI 52100 steel and attributed it to the tempering process of martensite resulting from thermal effects.

However, a limited number of studies have recognized the significant role played by severe plastic deformation in the formation of the white layer during hard-turning [8], [9], [20], [22], [23]. This scenario occurs when temperatures are insufficiently high for the

austenitization process to take place, typically due to low cutting speeds, low feed rates, and minimal tool wear. In such cases, mechanical deformation predominates in the white layer formation.

Ramesh et al. [22], investigated the white layer formation on hard-turned AISI 52100 steel using a low CBN content cutting insert. Machining with a low cutting speed of 91.4 m/min resulted in the white layer formation because of significant plastic deformation and the refinement of grains. The observed retained austenite content was decreased, which was attributed to either strain-induced transformation or tempering effects. Both these phenomena occurred during the hard-turning process with the low cutting speed. In contrast, the high cutting speed of 273.4 m/min resulted in a white layer caused due to reverse martensitic transformation with high retained austenite content. Barry and Byrne [8] reported similar trends when using fresh and worn inserts, the worn inserts led to an increase in surface temperature and resulted in a white layer with increased retained austenite content.

Han et al. [20] examined the cutting temperatures during orthogonal machining of AISI 1045 annealed steel and noted the development of a white layer below the phase transformation temperature, attributed to plastic deformation. Hosseini et al. [9] examined the formation mechanism of white layers using a low cutting speed of 30 m/min. They reported that no dark layer formed beneath the white layers and referred to them as mechanically induced white layers with lower retained austenite content than in the bulk. Additionally, TEM examinations unveiled elongated nano-sized grains within the mechanically induced white layer, a result of the dynamic recovery process.

Numerous studies conducted using TEM have found that the white layer comprises nanocrystalline grains ranging from <10 nm to submicron grains of 200 nm [8], [9], [23], [24]. Ramesh et al. [22] reported that the white layers formed by thermal domination had larger grains (~ 20 nm ) compared to the mechanical dominant white layer (~5 nm). Because of the ultra-fine grain size of the white layer, the hardness in this area exceeds that of the bulk material, primarily due to the Hall-Petch effect and dislocation strengthening. Zhang et al. [21] measured the hardness of the white layer and dark layer in comparison with the parent tempered martensite bulk material in AISI 52100 steel. The average hardness of the bulk material is around 10.3 GPa with the white layer being 12.5 GPa and the dark layer being 8.8 GPa. Ramesh et al. [22] reported that the increase in white layer hardness is observed with higher cutting speed as the dominant thermal phase transformation causes the carbon to be retained in the white layer due to carbide dissolution. However, when examining the hardness of the white layer in the EDM sample, which formed solely through reverse martensitic transformation, a decrease in hardness is noted in comparison with the hard-turned white layer, attributed to the formation of a high retained austenite content. Hosseini et al. [25] reported that the mechanically induced white layer displayed approximately 26% higher hardness than the bulk material, primarily due to severe plastic deformation that

led to the formation of subgrains, and under these circumstances, there is no formation of a softer dark layer beneath the white layer.

## 2.3 Formation mechanism

The metal-cutting process is characterized by the intense deformation of workpiece material within a small volume during short intervals. During this process, the material flow stress depends on the cutting process and workpiece properties. The factors depending on the cutting process are - strain, strain rate, and temperature. A few of the workpiece properties that affect the material flow stresses are initial grain size, crystal structure, hardening behaviour, specific heat etc. [26].

During conventional material tests, the strain rates typically range from $10^{-3}$ to $10^{-1}$ $s^{-1}$ (isothermal condition). The strain rates involved in machining operations are typically in the order of $10^{3}$ to $10^{6}$ $s^{-1}$ (adiabatic condition) and much higher compared to the isothermal conditions and strains ranging between 1 – 10 [26]. In the adiabatic condition, the strain rate determines the rate of heat generation during deformation and the thermal conductivity of the workpiece material controls the heat dissipation rate. In metallic materials experiencing strain rates exceeding $10^{2}$ $s^{-1}$, localized deformation accelerates, raising the temperature in the deformed area. This increase in temperature leads to a reduction in material flow stress due to thermal softening. Since heat generation from deformation outpaces heat dissipation rate, the material undergoes localized shear propagation, culminating in catastrophic failure [27]. Zener and Hollomon [28] were the first to identify adiabatic shear as the predominant factor contributing to the failure of metallic targets under high strain-rate ballistic impacts.

Depending on the cutting speeds and tool wear, the measured cutting temperatures during the white layer formation in hard-turning can be above or below the austenitization range. In their research, Ueda et al. [29] investigated the cutting temperatures in AISI 52100 steel (700 HV1) with a CBN insert. They found that at a cutting speed of 100 m/min, the temperature measured was 800 ºC, whereas at 300 m/min, the temperature on the cutting edge of the tool flank reached 950 ºC. According to Han et al. [20] despite the transformation temperature not being reached, they observed the formation of a white layer on the machined surface during the AISI 1045 orthogonal cutting. Similarly, Hosseini et al. [30] investigated the formation of white layers on hard-turned AISI 52100 steel and utilized a two-colour pyrometer technique to measure cutting temperatures. They found that thermally-induced white layers formed within the range of 840 ºC to 920 ºC. In contrast, mechanically-induced white layers formed at approximately 550 ºC, significantly below the austenitization temperature of 750 ºC.

Zhang et al. [31] examined the microstructures formed during impact wear testing of a low alloy carbon steel with an initial tempered martensite microstructure. Following testing, the material exhibited a surface white layer and internal white adiabatic shear

bands. TEM analysis revealed fine subgrains in both regions with no FCC diffraction patterns observed. They concluded that the formation of surface white layers and internal adiabatic shear bands were attributed to the dynamic recovery process. Barry and Byrne [8] conducted a study on the formation of white layers in AISI 4340 tempered martensite steel using both unworn and worn tools. They proposed that when unworn tools were used, dynamic recovery acted as the initiation mechanism for the refined structure, similar to the internal adiabatic shear bands (ASB) mechanism. However, when worn tools were employed, the increased temperature on the workpiece led to dynamic recrystallization dominating the process, resulting in a very fine grain structure with increased FCC content.

From the previous studies, the nanocrystalline structures observed in the white layers during hard-turning with high strain-rate conditions are either the result of a dynamic recovery mechanism due to severe plastic deformation at low cutting speeds or dynamic recrystallization mechanisms in combination with severe plastic deformation and reverse martensitic transformations at high cutting speeds [8], [9], [22], [23].

### 2.3.1 Dynamic recovery and dynamic recrystallization

The hot working behaviour of alloys is typically observed by flow curves, which are a direct result of changes in microstructure: a) work hardening, b) dynamic recovery and c) dynamic recrystallization [32].

During the thermo-plastic deformation, the crystalline material's free energy is increased by an increase in the dislocation density due to deformation, which results in the work hardening phenomenon on the flow stress. In this stage, the morphology of the grains remains the same due to relatively low plastic strain. As the deformation progresses, adiabatic shear is initiated, leading to a sharp increase in dislocation density. It is believed that the material containing those flaws is thermodynamically metastable. Further, the intense plastic shear results in the reorientation and elongation of the grain structure along the shear direction. As deformation localization intensifies, dislocations start climbing to form dislocation cells. The dynamic recovery process initiates with the annihilation and rearrangement of dislocations. In such scenarios, the rate of defect generation (dislocation increase) exceeds that of dislocation annihilation. Consequently, only partial elimination of dislocations occurs under these conditions. With the assistance of the local temperature rise resulting from localized plastic deformation, dislocation tangles are generated, creating areas with varying dislocation densities and forming subgrain boundaries. The subgrain cell walls subsequently segment, leading to the refinement of elongated grains [31], [32], [33], [34]. Dislocation climb is a crucial mechanism for dynamic recovery. In metals characterized by high stacking fault energy (SFE), dislocation climb happens quickly. Conversely, metals with low SFE experience challenges in dislocation climb out of their glide planes. Alloys exhibiting slow dynamic recovery due to low SFE are more prone to undergo dynamic recrystallization [8], [35].

The substantial strain energy stored in the deformed elongated grains notably lowers the recrystallization temperature. Additionally, the intense plastic deformation at high strain rates contributes to an increase in the workpiece temperature [36]. When the stored energy surpasses a critical threshold where the work hardening and recovery can no longer store immobile dislocations, a more intense restoration process known as dynamic recrystallization inevitably takes place usually in low SFE materials. This process involves the formation of new dislocation-free grains within the deformed or recovered structures. These new refined equiaxed grains then grow and consume the old grains, leading to a new grain structure with a comparatively lower dislocation density. However, if deformation persists, the dislocations in the newly formed grains will continue to increase [32], [34]. At 1000 ºC, BCC iron has a high SFE of 0.2 $Jm^{-2}$ in comparison to the FCC iron of 0.075 $Jm^{-2}$ SFE. The low SFE of FCC iron formed due to reverse martensitic transformation favors the occurrence of dynamic recrystallization [8].

# CHAPTER 3

# Materials

## 3.1 AISI 52100 workpiece material

The workpiece material investigated in the scope of this work is high carbon-chromium steel SAE/ASTM/AISI 52100 (DIN 100Cr6, SUJ2, EN31) in tempered martensitic condition. This material is widely used in bearing industries due to its high wear resistance, and high strength properties to withstand heavy rolling contact fatigue loadings [37]. The nominal composition is provided in Table 1.

*Table 1: Chemical composition of 52100 steel used in the current study, Fe-bal.*

| Element | C | Mn | Cr | Si | S | P |
|---|---|---|---|---|---|---|
| Wt.% | 0.95 | 0.32 | 1.42 | 0.26 | 0.001 | 0.009 |

The initial state of AISI 52100 steel is spheroidize annealed, characterized by finely dispersed cementite precipitates in a nearly spherical form within the ferrite matrix. This microstructure typically exhibits a hardness of approximately 200 HV. The spheroidization process involves chromium partitioning into the cementite ((Fe, Cr)3C), leading to a microstructure that facilitates efficient machining [38]. The hardness requirement for bearing components is typically around 700 HV (58 HRC – 62 HRC) [39]. To attain these final properties, the steel undergoes a through-hardening heat treatment process. This process begins with austenitization at approximately 840 °C, followed by rapid quenching in oil to achieve a martensitic microstructure.

Subsequently, tempering (between 1st and 2nd stages) is carried out to reduce the retained austenite (RA) content to below 2% and achieve a final hardness of approximately 58 – 60 HRC. After the through-hardening heat treatment process, the microstructure comprises a combination of plate and lath tempered martensite matrix, along with tempered cementite and near-spherical (Fe, Cr)3C cementite, with less than 2% retained austenite as shown in Figure 3 below [40], [41].

Depending on the application, the microstructure is optimized concerning retained austenite content, and carbide fractions distribution in the microstructure. In this thesis, the study also focused on the role of retained austenite content in the white layer formation. Two different retained austenite contents (12% and 25%) were obtained by varying the heat treatment process in the AISI 52100 steel.

To obtain a retained austenite (RA) content of 12%, batch 1 samples underwent austenitization at 860 °C for 120 minutes with a carbon potential of 0.75% in the furnace. On the other hand, to obtain 25% RA, batch 2 samples were austenitized at 920 °C with a carbon potential of 0.8% in the furnace for the same duration. Maintaining the carbon potential is crucial to prevent decarburization caused by the higher austenitization temperature. Both batches were then quenched in oil at 80 °C, with the samples oriented vertically to ensure uniformity. Following quenching, both batches underwent tempering at 160 °C (1st stage) for 60 minutes. The final hardness achieved was within the range of 61±2 HRC.

Increased austenitizing temperatures can lead to a higher volume fraction of retained austenite primarily due to the increased carbon content in the austenite phase. This higher carbon content helps to stabilize the retained austenite, preventing its transformation into martensite during quenching by lowering the martensite transformation temperature. By varying the austenitization temperature, different volume fractions of retained austenite can be achieved [42], [43].

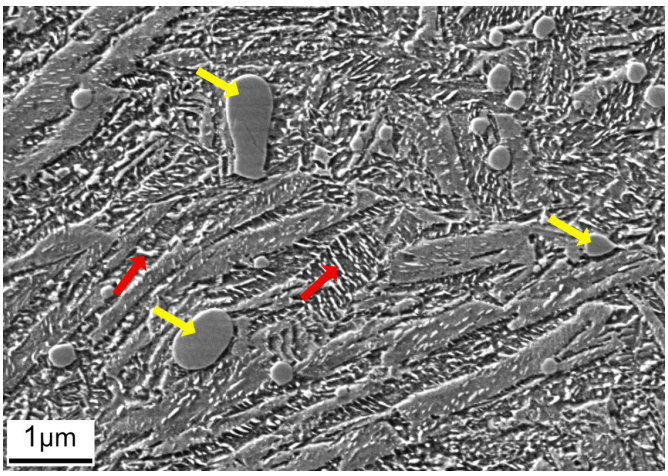


*Figure 3: SEM image of the bulk tempered martensite microstructure. Yellow arrows indicate the (Fe, Cr)$_3$C carbides in the matrix and red arrows indicate the tempered cementite within the martensite.*

## 3.2 Martensite

The term "martensite" was coined in 1890 as a tribute to the contributions of Adolf Martens, specifically to describe the hard phase observed in steel that underwent rapid cooling. However, in contemporary usage, it refers more broadly to any diffusionless transformation that emerges during cooling or deformation processes in ferrous, nonferrous materials and ceramics [44].

Martensite is formed when austenite undergoes rapid cooling at speeds exceeding the diffusion rate of carbon atoms. Martensitic transformation in steel has been observed to occur at a speed of 1000 $ms^{-1}$ [45]. When diffusion is inhibited, carbon atoms are unable to escape and become trapped at octahedral sites within the face-centered cubic (FCC) austenite lattice. This trapping induces the transformation to the body-centered tetragonal (BCT) lattice of martensite through a diffusionless shear process. There is a coordinated shift that results in atomic movements that are less than the interatomic distance. The significant disparity in solubility between FCC and BCT structures results in the BCT lattice of martensite being supersaturated with carbon, leading to lattice distortions [45]. The lattice parameters change proportionally with the carbon content, and this relationship can be expressed by the ratio of the axes, c/a, as indicated in equation 1.

$$\frac{c}{a} = 1 + 0.045 * wt.\,\%\,C \qquad (1)$$

In this equation, c and a represent the axes of the body-centered tetragonal (BCT) unit cell.

Martensite formation is diffusionless and athermal, so the level of undercooling determines the extent of transformation. The temperature at which martensite formation starts is called the martensite start temperature ($M_s$), indicating the necessary energy for austenite-to-martensite transformation. Conversely, the martensite finish temperature ($M_f$) marks the end of martensite formation, beyond which further cooling doesn't lead to martensite formation. With higher carbon content, martensite transformation temperatures decrease as carbon strengthens the resistance of austenite to shear. In cases of high carbon content, complete martensite transformation might not happen at room temperature, leading to retained austenite formation [45], [46].

Martensite primarily takes two forms: lath martensite and plate martensite. The type of morphology formed depends on the carbon content present. Lath martensite is typically observed when the carbon content is $\leq$ 0.6 wt.% C, whereas plate martensite is seen when the carbon content is $\geq$ 1 wt.% C. In cases where the carbon content falls between these values, a combination of lath and plate martensite may be observed [45].

After rapid cooling, martensite becomes hard and brittle, resulting in a material with reduced toughness and ductility. To address this, bearing steels often undergo

additional tempering. This process involves heating the material to a temperature above room temperature but below the $A_{C1}$ point for a specific duration. Under these conditions, martensite is highly susceptible to phase transformations due to: (i) the dense dislocations and martensite crystal interfaces, which promote grain recovery and growth, (ii) the supersaturation of alloying elements, leading to segregation and carbide precipitation, and (iii) the presence of unstable retained austenite below the $A_{C1}$ point [47]. Distinct stages related to specific microstructural changes have been identified based on both time and tempering temperature [41], [45], [47].

- *Segregation (T < 100 ºC):* carbon atoms migrate towards dislocations, with up to 0.2 wt. %C is involved in the migration.
- *First stage (100 ºC < T < 200 ºC):* precipitation of nano-sized transition ε-carbides and η-carbides with a partial loss of tetragonality.
- *Second stage (200 ºC < T < 300 ºC):* decomposition of retained austenite to form cementite and ferrite.
- *Third stage (250 ºC < T < 350 ºC):* precipitation of cementite ($Fe_3C$) to the detriment of existing ε-carbides.
- *Fourth stage (350 ºC < T < $A_{C1}$ ):* recovery, martensite lath coarsening and recrystallization.

By carefully varying the austenitization and tempering temperatures, it is possible to achieve a final microstructure of tempered martensite that maintains the high strength of martensite while also retaining a certain level of ductility and toughness with different retained austenite content.

# CHAPTER 4

# Hard Turning

## 4.1 Introduction

The fundamental goal of metal cutting processes is to create a fresh surface with the required surface integrity on the workpiece by mechanically eliminating the material in the form of chips. This objective can be accomplished using tools featuring single-point (turning) or multi-point (milling) geometrically defined cutting edges or tools with geometrically undefined cutting edges (such as grinding). This work specifically emphasises hard turning, a process employing a single-point, geometrically well-defined cutting edge to machine metallic materials with a hardness exceeding 45 HRC [1].

## 4.2 Fundamentals of hard-turning

### 4.2.1 Cutting parameters

The underlying principle for generating the machined surface relies on ensuring the appropriate relative motion between the workpiece and the cutting tool. In hard-turning, the workpiece is held in a rotating chuck while the cutting tool moves along its surface, resulting in the formation of chips due to their relative motion. This process, where the tool is fed along the length of the workpiece parallel to its axis of rotation, is referred to as longitudinal turning as illustrated in Figure 4 [48].

The primary group of cutting parameters critical for machining processes includes cutting speed ($v_c$), feed rate ($f$), and depth of cut ($a_p$). Cutting speed refers to the relative velocity between the workpiece and the cutting tool, usually stated in meters per minute (m/min). Feed rate indicates the distance travelled by the cutting tool for each revolution of the workpiece, measured in millimetres per revolution (mm/rev), while the depth of cut is the depth to which material is removed, expressed in millimetres (mm). Figure 4 illustrates the key process parameters.

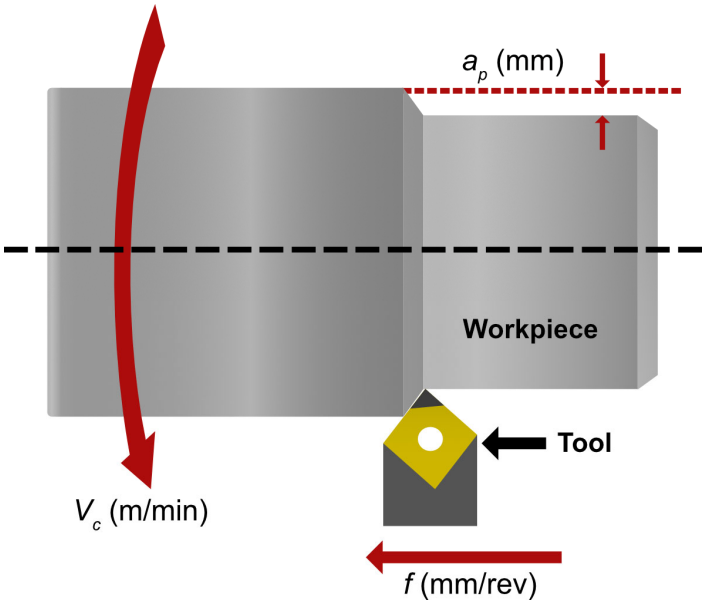


*Figure 4: Illustration of the longitudinal hard-turning process. Key process parameters cutting speed ($v_c$), feed rate ($f$), and depth of cut ($a_p$) are indicated along with the workpiece, and tool direction.*

### 4.2.2 Heat generation and deformation zones

Roughly 97% of the mechanical energy is transformed into thermal energy during the hard-turning process through the workpiece plastic deformation and the frictional work taking place at the interface between the workpiece and the tool. The three shear zones—primary, secondary, and tertiary zones—are where heat is generated and then transported to the workpiece, tool, and chip as shown in Figure 5. In the primary zone (*I*), material from the workpiece is sheared off to create chips. The zone extends from the cutting tool tip to the point where the undeformed workpiece surface intersects with the deformed chip. Heat is generated in this area from plastic deformation, leading to material softening and increased deformation. Approximately 80% of the heat is produced in the primary shear zone, of which 75% is removed through the chip and 5% is transferred to the workpiece. The secondary shear zone (*II*) occurs at the tool rake face-chip interface. Heat is produced in this zone through the plastic deformation of the chip and the friction between the tool's rake face-chip interface. Of the remaining 20% thermal energy, 18% is produced at the secondary zone. The tertiary shear zone (*III*) arises in the freshly machined surface under the tensile stress exerted by the tool's

clearance face. The remaining 2% heat is generated here through the plastic deformation of the fresh surface and the frictional work between the clearance face and the newly generated surface [49], [50].

During the cutting process, the material in front of the cutting tool tip is either displaced upwards by the rake face to form a chip or ploughed below the cutting edge to create the machined surface. The point where the material flow diverges to create the chip and the newly machined surface is known as the stagnation point as shown in Figure 5 [50].

The friction and temperature at the tool-workpiece and tool-chip interfaces contribute to the progression of tool wear through various simultaneous mechanisms, ultimately leading to compromised surface integrity. To mitigate these negative effects, cutting fluids are employed to reduce friction and heat during tool and workpiece interaction. The application of coolant in hard-turning offers three major beneficial effects: a) cooling, b) lubrication between the chip and rake face, and c) efficient chip removal from the workpiece [49].

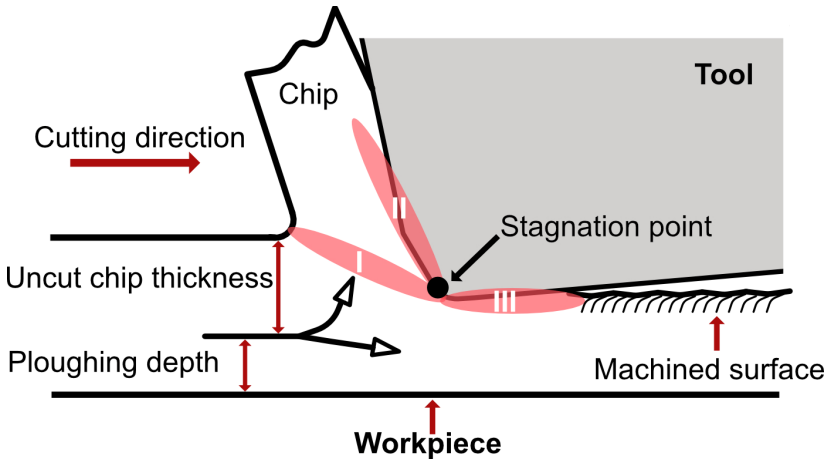


*Figure 5: Schematic illustration of the deformation zones: Primary shear zone (I), Secondary shear zone (II), and Tertiary shear zone (III). The stagnation point is indicated in the image where the material flow separates to form the chip and machined surface.*

## 4.3 Cutting tool

The cutting tools used in hard-turning must endure significant mechanical forces and high temperatures simultaneously. Moreover, the friction between the tool and chip, as well as between the tool and workpiece, is substantial. To execute hard-turning effectively, the tool must exhibit characteristics like high wear resistance, elevated temperature hot hardness, increased toughness to prevent fractures, and stability both chemically and physically at high temperatures [51].

The introduction of polycrystalline cubic boron nitride (PCBN) cutting tools, comprising sintered CBN grains with a binder, has revolutionized hard-turning. Coating

these PCBN inserts and developing the required tool geometry has enhanced cutting tool performance by reducing wear, thereby extending the tool lifespan and ensuring the desired surface quality on the workpiece [49]. Figure 6 illustrates the schematic representation of the cutting tool geometry utilized in the thesis work.

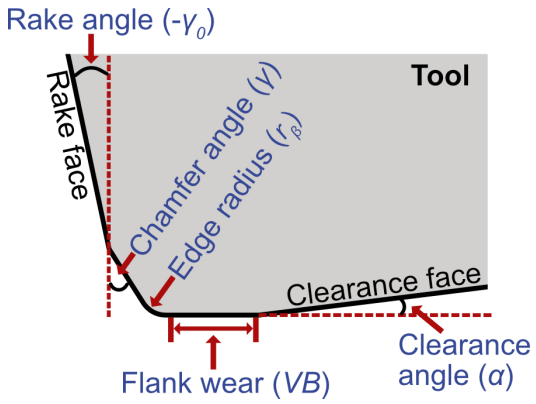


*Figure 6: Cutting tool geometry with important features.*

### 4.3.1 Tool wear

Despite its ability to produce surface integrity comparable to that of a ground workpiece in a shorter production time, hard-turning is not widely adopted as the final finishing process. This is primarily because the cutting tool experiences continuous deterioration, resulting in significant tool wear that directly affects the workpiece's surface integrity. As the tool wear progresses, cutting forces and temperatures rise due to the increased contact length during machining between the cutting tool and workpiece. The degradation of tools can be categorized based on micro and macro scale progression into two main groups: wear and fracture [52].

The wear mechanism in the cutting zone becomes intricate due to the simultaneous influence of mechanical, thermal, and adhesion factors. Because of these factors, tool wear can be caused by multiple mechanisms or specific mechanisms depending on the cutting conditions. The four primary classifications of wear mechanisms are: a) abrasive wear, b) adhesion wear, c) diffusion wear, and d) chemical wear. When cutting speeds are low to moderate, mechanically dominated abrasive and adhesive wear tends to dominate. Conversely, at high cutting speeds, thermally activated diffusion wear, thermal wear (caused by plastic deformation due to thermal softening), and chemical wear (resulting from oxidation and corrosion) become the dominant mechanisms [49], [52].

Due to the continuous action of the chip removal process by the cutting tool, the tool wear can be located in two zones:

- The wear on the rake face is identified by the formation of a crater or built-up edge, which occurs due to the action of chip flow along the rake face. Its primary cause is due to adhesion and diffusion.
- Wear on the flank or clearance face results from the high friction between the tool edge and the newly machined surface, with abrasion being the primary wear mechanism.

Figure 7 (a) represents the fresh cutting insert with a 15° chamfer angle after machining with VB: ~ 0.04 mm and Fig. 7 (b) shows a pre-worn insert with a 35° chamfer angle after machining with VB: ~ 0.21 mm. Flank wear and crater wear are observed on the worn insert which eventually affects the surface integrity.

In hard-turning operations, flank wear (*VB*) is the preferred mode of tool wear pattern as it affects the surface quality due to its gradual progression and controllability. The thesis is focused on investigating the impact of flank wear on residual stresses, surface roughness, and white layer generation in comparison to the fresh inserts.

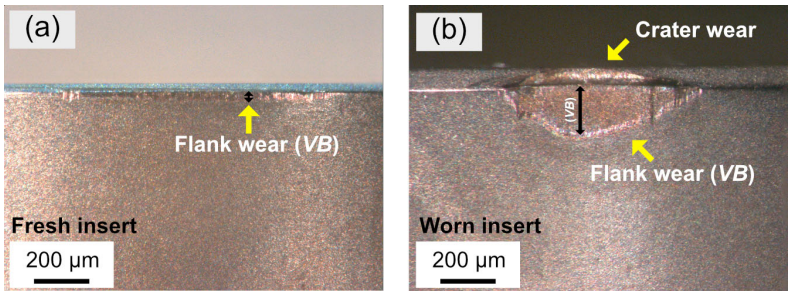


*Figure 7: (a) Fresh insert after machining observed VB: ~0,04 mm flank wear (15° chamfer angle) (b) Pre-worn insert after machining with VB: ~ 0.21 mm (35° chamfer angle) and crater wear is observed on the rake face.*

### 4.3.2 Tool geometry

Cutting tool geometry significantly impacts the hard-turning process. A crucial aspect of hard-turning is selecting the suitable rake angle and preparing the cutting edge correctly. When machining hardened steel, a negative rake angle is preferred by aligning the tool along the cutting speed direction. Additionally, a positive clearance angle between the tool and the workpiece is maintained to avoid rubbing against the workpiece during cutting. This setup ensures a robust cutting edge, reducing the risk of chipping under high cutting forces. A chamfer is incorporated into the tool's cutting-edge design to withstand the significant tool stresses that are generated during machining [49], [53]. Tool geometry including tool nose radius, edge radius, and chamfer angle, when combined with cutting parameters like cutting speed, feed rate, and depth of cut, plays a crucial role in influencing residual stress generation, surface roughness, and white layer microstructural evolution on the machined surface after hard turning. The surface integrity of these parameters is discussed in section 4.4.

## 4.4 Surface integrity

Surface integrity involves examining the changes that occur during the manufacturing process of a component, which can impact its properties and overall service performance. The term surface integrity is defined as '*The inherent or enhanced condition of a surface produced in machining or other surface generation*' [54]. Considering that components undergo dynamic loads after hard-turning, surface integrity can be divided into two main aspects and holds great significance [55], [56].

- Geometric irregularities (surface finish and texture)
- Internal subsurface aspects (metallurgy, hardness, and residual stresses)

In this section, the theory of surface topography and residual stresses are discussed. White layer metallurgical features and their corresponding hardness effects were discussed in Chapter 2.

**Surface topography**: Surface topography results from a combination of factors, including aspects of the manufacturing process and characteristics of the workpiece material. Topography irregularities arise from a combination of three types of features: surface form, surface waviness, and surface roughness. Form and waviness are caused by macrogeometric errors like cutting tool instability and workpiece deflection, while roughness pertains to microgeometric errors. The current work is focused on evaluating the surface roughness generated with varied cutting conditions. Surface roughness is defined as the high-frequency irregularities on a surface, which emerge from the interaction between the cutting tool parameters and the workpiece microstructure [55]. The surface roughness achieved after hard-turning is primarily influenced by tool geometry, cutting speed, and feed rate. However, factors such as the built-up-edge phenomenon, tool wear and machine-tool dynamics also play crucial roles in determining the surface texture quality.

**Residual Stresses:** Residual stresses are internal stresses that maintain equilibrium within components without the influence of external forces, and thermal gradients. Depending on the length scale, the residual stresses are classified into macro residual stresses that balance throughout the bulk of the material (Type I). Micro residual stresses are equilibrated among grains and can vary due to the presence of different phases within the material (Type II). Sub-micro residual stresses occur at atomic dimensions within a grain, where they balance due to line defects (dislocations) and point defects (vacancies and interstitials) in the solid body (Type III). All types of residual stresses are present to some extent in the components [57].

The residual stress distribution in machined components is influenced by both the machining process parameters and the preceding materials processing steps. The combination of thermal and mechanical effects during the hard-turning generates the residual stresses in the machined component. The residual stress state in machined surfaces can be attributed to several factors, including [55]:

- The pressure between the tool and the workpiece causes rubbing, leading to plastic deformation of the machined workpiece material and consequently generating compressive residual stresses.
- Tool/workpiece friction during plastic deformation heats the surface, causing temporary expansion due to the surrounding material's constraints. This can exceed the yield stress, leading to plastic deformation. Subsequent cooling induces thermal contraction, resulting in tensile residual stresses at the surface.
- Elevated cutting temperatures can trigger phase transformations in the machined material. For instance, in hardenable steel, rapid heating, and cooling can generate martensite, creating compressive stresses due to volumetric changes during the transformation.

### 4.4.1 Influence of cutting parameters and tool geometry on surface integrity

The impact of cutting parameters and tool geometry on surface integrity has garnered significant research attention, resulting in varied findings across the literature.

Navas et al. [58] studied the impact of feed rate on surface residual stresses in AISI 4340 steel. They found that increasing the feed rate led to higher surface tensile stresses, attributed to the elevated temperature during cutting. This temperature rise was linked to increased chip thickness, generating more heat from material plastic deformation during chip formation and contributing to thermal tensile stresses on the surface. Dahlman et al. [59] investigated how rake angle, and cutting feed influence residual stresses during the hard turning of AISI 52100. They found that higher feed rates and more negative rake angles led to increased compressive stresses beneath the surface. A more negative rake angle leads to increased mechanical action in the subsurface, resulting in higher compressive stresses due to the rise in passive cutting force [60]. Higher feed rates lead to elevated temperatures, causing increased tensile plastic deformation below the cutting tool (beneath the flank face). This deformation region deepens with the feed rate. As a result, at higher feed rates, the tensile plastic deformation extends further under the flank face behind the cutting edge. When the deformation zone is unloaded, this leads to a reversal in the stress state, creating deeper compressive residual stresses [60], [61], [62]. The effect of cutting speed on residual stresses was reported by Gunnberg et al. [60] in hard-turned case-carburized 18MnCr5 steel using a PCBN cutting tool. They observed that the increased cutting speed generates more heat, leading to higher temperatures and surface tensile residual stress. However, because most of the heat is removed by the chip, the high temperature does not penetrate deeply into the workpiece, limiting its impact on residual stress generation below the surface. Dahlman et al. [59], Gunnberg et al. [60], and Matsumoto et al. [63] reported that the impact of depth of cut on residual stresses in hard-turning was minimal. Abräo et al. [64] investigated the impact of tool wear on residual stresses generated in AISI 52100. They observed that worn inserts resulted in higher compressive

stresses at a depth of 20 µm from the surface. This is because worn inserts require higher cutting forces to shear the material, leading to the induction of compressive stresses, in contrast to the lower mechanical energy required with sharp inserts. Liu et al. [65] studied how tool wear impacts residual stress formation in SuJ2-bearing steel during hard turning. Their findings indicate that as tool wear increases, surface tensile stresses and compressive residual stresses beneath the surface are observed. This outcome is attributed to higher thermal energy resulting from friction and plastic deformation on the machined surface due to tool wear. The increased friction amplifies thermal energy, subsequently raising surface temperatures. Moreover, higher thrust force due to a larger contact area leads to more significant mechanical impacts beneath the surface. König et al. [66] also observed similar effects regarding the impact of tool wear on residual stresses. Hua et al. [62] examined how the hone radius and chamfer angle of a cutting tool affect subsurface residual stresses during the hard-turning of AISI 52100 steel. They found that incorporating a chamfer with the hone radius enhanced the rounding of the cutting edge, resulting in increased subsurface compressive stresses. Increasing the hone radius and chamfer angle results in burnishing at the cutting edge, which becomes a prominent factor in chip formation. This burnishing process, involving the material being squeezed under the cutting edge, leads to significant elastic and plastic deformation on the machined surface, resulting in higher compressive residual stress levels. Varela et al. [67] noted similar effects with the chamfer+honing edge geometry. This geometry resulted in higher negative rake angles, which in turn increased cutting forces and generated higher compressive stresses.

The surface roughness of hard-turned components is significantly influenced by the feed rate and tool nose radius, which are widely recognized as the main parameters in this context. A theoretical model for machining surface roughness ($R_a$) with $f$ as feed rate (mm/rev) and $R_\varepsilon$ as tool nose radius (mm) is given in equation 2:

$$R_a = \frac{f^2}{32R\varepsilon} \quad (2)$$

According to this equation, the calculated surface roughness tends to be higher or lower than the experimental values. This discrepancy could be attributed to the material's plastic flow caused by the hone edge geometry as this equation does not incorporate tool geometry.

Increasing the feed rates with a constant tool nose radius increases the surface roughness as the higher feed rate increases the separation between the feed marks. Benga et al. [68] investigated the impact of feed rate and cutting speed on surface roughness in 100Cr6-bearing steel (AISI 52100). They noted that lower feed rates led to smoother surfaces due to the reduced distance between peaks and valleys on the machined surface. The optimal cutting speed range of 116 – 130 m/min produced the best surface roughness. Below this range, insufficient temperature did not reduce the workpiece's shear strength, requiring higher cutting forces that worsened surface roughness. Conversely, speeds above this range caused machine/tool vibrations and

increased tool wear resulting in higher surface roughness. Expanding the edge hone radius under a constant feed rate generally increases average surface roughness. This occurs due to a greater contribution from the deformation ploughing component than the shearing component [69]. The honed radius significantly impacts side plastic flow compared to chamfer geometry. During cutting, a higher negative rake angle and lower feed rates lead to increased material interaction with the cutting edge. This causes material displacement towards the side of the cutting edge, resulting in plastic deformation at elevated temperatures, resembling a viscous liquid behaviour. The plastically deformed material is then pushed out of the cutting-edge region as side flow. Consequently, this mechanism raises peak heights in the cut profile, increasing surface roughness. This mechanism is absent in chamfered tools without hones, aligning the surface roughness more closely with theoretical values. While tool edge geometry is crucial for surface roughness, feed rate remains the dominant factor [67], [70].

# CHAPTER 5

# Methodology and Material Characterization

In this chapter, the methodology and characterization techniques are explained. Paper A and Paper B examine research question 1 and Paper C examines research question 2.

## 5.1 Methodology

The longitudinal hard-turning machining experiments were performed using MONFORTS RNC500 Single Turn machine (Paper A and Paper B) and Hembrug CNC turning machine (Paper C) in wet conditions. Cylindrical rings with dimensions 180 mm diameter and 60 mm length were machined and investigated in papers A and B. For Paper C, cylindrical rods with a length of 200 mm and a diameter of 34 mm were machined and analysed.

To understand the effects of cutting parameters on the white layer formation and its impact on surface integrity (Paper A and B), cutting speed ($V_c$), feed rate ($f$), depth of cut ($a_p$), coolant pressure ($P$), tool chamfer angle ($\gamma$), and tool wear ($VB$) are varied between two levels as mentioned in Table 2. The full factorial design of experiments resulted in 64 tests. Tool wear ($VB$) of 0.2 mm signifies that the tool needs pre-treatment to run the experiment. As part of the pre-treatment, a new tool was used to machine the extra workpiece with a cutting speed ($V_c$) of 110 m/min until the tool flank wear (VB) reached 0.2 mm in a controlled manner under identical conditions of feed rate ($f$), depth of cut ($a_p$), and chamfer angle ($\gamma$). While generating the flank wear, crater wear is also observed on the tool rake face. The current study specifically focuses on flank wear's impact, given its significant influence on white layer formation compared to crater wear.

*Table 2: Test parameters to understand the effect of cutting parameters on the white layer formation and its impact on surface integrity (Paper A and Paper B).*

| Parameters | Units | Low | High |
|---|---|---|---|
| Cutting speed ($V_c$) | m/min | 60 | 110 |
| Feed rate ($f$) | mm/rev | 0,05 | 0,2 |
| Depth of cut ($a_p$) | mm | 0,05 | 0,2 |
| Coolant pressure ($P$) | bar | 20 | 150 |
| Chamfer angle ($\gamma$) | deg | 15 | 35 |
| Tool wear ($VB$) | mm | 0 | ~0,2 |

To investigate the impact of retained austenite content on white layer formation and residual stress distribution (Paper C), the study varies the cutting speed ($V_c$) and flank wear ($VB$) according to the depicted Figure 8. The feed rate ($f$) is maintained at 0.16 mm/rev, and the depth of cut ($a_p$) is kept constant at 0.16 mm under wet conditions with flooding coolant. The design of experiments resulted in 12 tests.

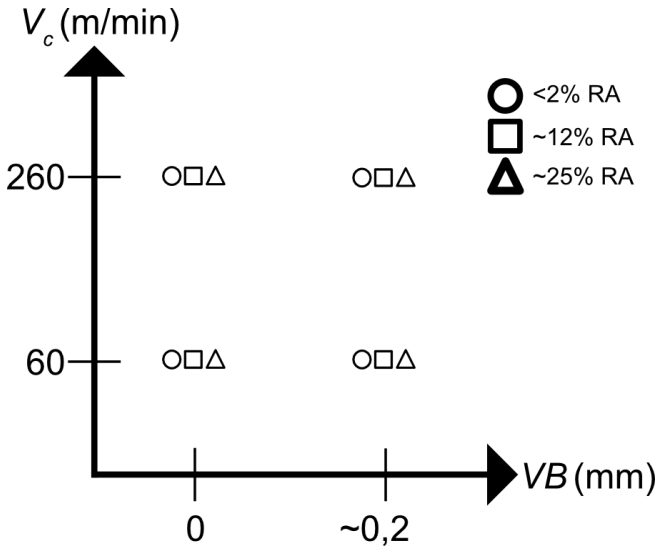


*Figure 8: Test parameters to study the role of retained austenite in the white layer formation (Paper C).*

Two different grades of coated polycrystalline cubic boron nitride (PCBN) cutting inserts are used to perform the hard-turning experiments. BNC 2125 (DNGA 1506 S01015/S01035) cutting insert is used in papers A and B. BNC 200 (DNGA 150612 (HS)) cutting insert is used in paper C. The tool nose radius is varied for 2 cutting inserts. Table 3 shows the cutting insert specification for BNC 2125 and BNC 200.

*Table 3: Cutting tool specifications. BNC 2125 (paper A and Paper B), BNC 200 (Paper C).*

| Cutting inserts | BNC 2125 | BNC 200 |
|---|---|---|
| CBN content (%) | 65-70 | 65-70 |
| Coating | TiAlBN | TiAlN |
| Nose radius (mm) | 2 | 1.2 |
| Chamfer angle ($\gamma$) | $15^0$ / $35^0$ | $15^0$ |
| Chamfer land (mm) | 0.1 | 0.1 |

## 5.2 Material Characterization

After conducting the hard-turning tests, the surfaces of the machined components are thoroughly examined to assess the formation of white layers and their surface integrity. The techniques include X-ray diffraction (XRD) analysis for studying residual stresses, followed by measurements of surface roughness. The samples undergo sectioning, mounting, and polishing to enable observation of the white layers in the machined cross-section. Initial imaging using a light optical microscope (LOM) is carried out, followed by scanning electron microscopy (SEM) on the etched samples. Additionally, stereo optical microscopy (SOM) is conducted to examine the wear of cutting inserts, as the geometry of flank wear can impact surface roughness. Moreover, nanoindentation is performed on the white layer samples to determine their hardness. Figure 9 illustrates the hard-turned samples followed by the characterization techniques performed in the thesis work.

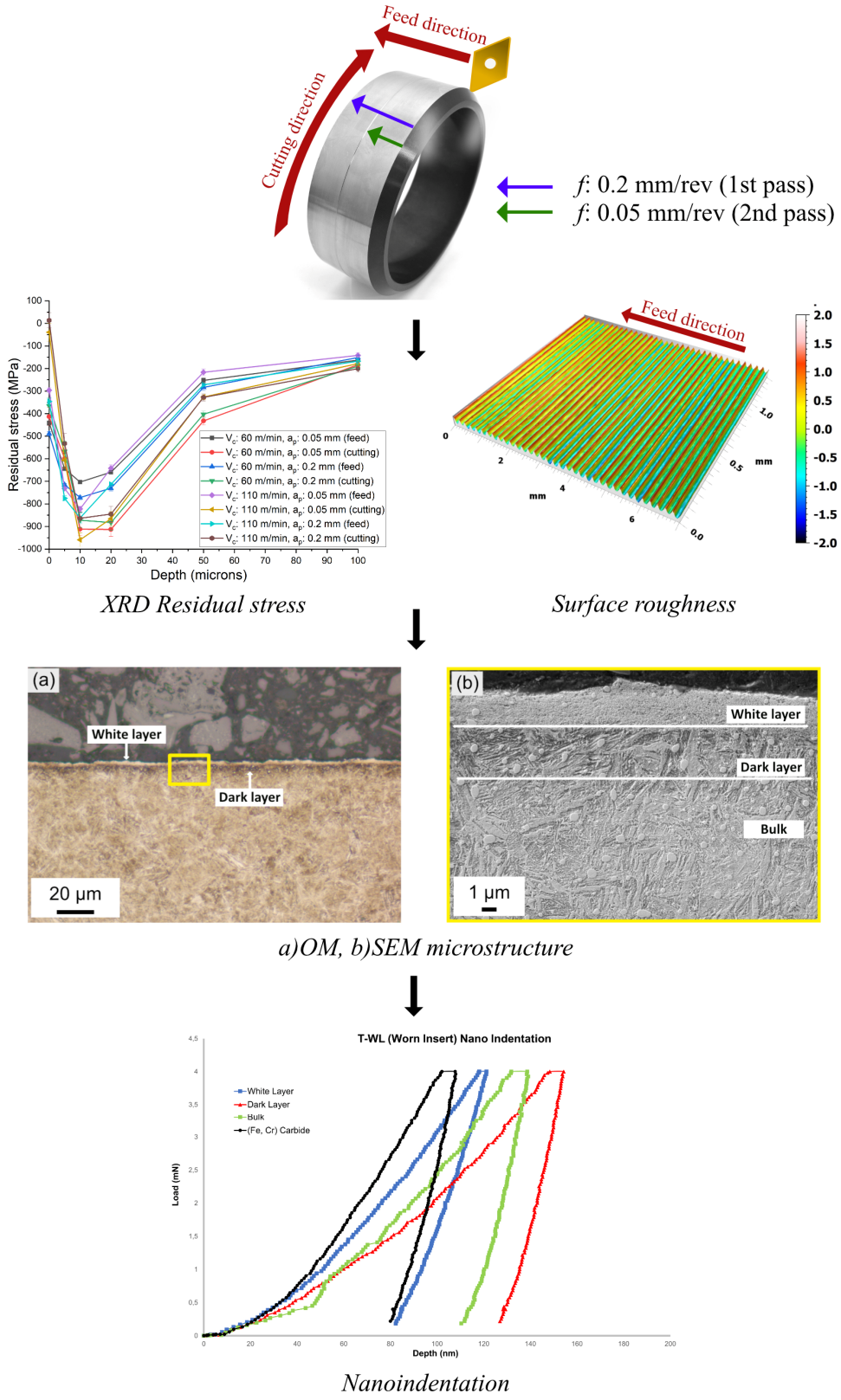


*Figure 9: Illustration of the hard-turning machining and the characterization techniques implemented in the thesis work.*

### 5.2.1 X-Ray diffraction

The X-ray diffraction (XRD) technique was used to measure the residual stresses generated by the hard-turning process (Paper A-C). Stresstech Xstress G2R 3000 laboratory XRD equipment was used. A Cr Kα X-ray tube with a wavelength (λ) of 1.54 nm and a 2 mm collimator was employed to measure the interplanar spacing of the crystal lattice. The XRD was operated at a voltage of 30 kV and a current of 9 mA. The tilt angles (ψ) spanned from -45° to +45°. Two position-sensitive detectors (PSD) were positioned on arc-shaped detectors at a 156.4° diffraction angle to measure the (211) lattice plane spacings utilizing the modified $\sin^2\psi$ method depending on the peak position using Bragg's law. Residual stresses were determined using elastic strain theory, where strain within the crystal structure was measured. Hooke's law was applied with Young's modulus of 210 GPa and Poisson's ratio of 0.3, both taken as tabulated values. Evaluation of residual stresses was conducted along the feed direction and cutting direction on the machined rings. The depth profile ranged from the surface to 100 µm (0, 5, 10, 20, 50, 100) below the machined surface. These measurements necessitated layer removal using electropolishing with a salt electrolyte, alongside a dial gauge to measure the depth removed.

When irradiated by X-rays, the sample undergoes an interaction with its atomic lattice. This interaction leads to the ejection of an electron from the outer shell, thereby producing a scattered X-ray beam. Those scattered X-rays that correspond to Bragg's law, expressed in equation 3, will be detected as a diffraction peak originating from a specific lattice plane by the detectors. The diffraction order is denoted by $n$, $\lambda$ represents the wavelength, $d$ stands for the interplanar spacing, and $\theta$ signifies the incidence angle.

$$n\lambda = 2dsin\theta \quad (3)$$

When a metal experiences stress, it undergoes elongation and contraction, causing changes in the interplanar spacing (d) of its crystal lattice. These alterations in lattice spacing correspondingly affect the diffraction angle (2θ). Precise measurement of this angle allows for the evaluation of the change in interplanar spacing, which in turn helps to measure the strain within the material. The d was plotted against several $\sin^2\psi$ tilt angles. From this measurement, the total stress on the metal can be determined using elastic theory equation 4, where m is the gradient of the d vs $\sin^2\psi$ line, E and ν are Young's modulus, and Poisson's ratio of the material.

$$\sigma_{\Phi} = (\frac{E}{1+\nu})m \quad (4)$$

### 5.2.2 Surface roughness

Surface roughness on the machined surface was evaluated using the Sensofar S Neox 3D optical profilometer equipment with coherence scanning interferometry technique (Paper A and Paper B). Interferometric microscopy is an optical technique used for non-

contact measurements of surface topography. The measurement covered a stitched area of 7.4 x 1.3 mm with a magnification of 20x and a uniform lateral resolution of 1.29 µm. Analysis of the acquired data involved applying a 2nd-order polynomial fit to remove form errors. To minimize short-wavelength noise, a spatial medium noise reduction filter was applied with a window size of 5 x 5 points. 3 measurements were performed on the samples and the results are averaged. The collected data was analyzed using Digital Surf's MountainsMap software. The roughness parameter ($R_a$) was evaluated in this thesis work.

### 5.2.3 Sample preparation

To conduct further analyses, cross-sectional samples are prepared. The machined workpieces are cut into smaller sections using a Struers cutting machine and then hot-mounted in conducting polyfast bakelite using CitoPress 20. The grinding process begins with P220 silica carbide papers with a coarser grit size. Subsequently, polishing is carried out on Struers Tegrapol machine using diamond-paste suspensions on 9 µm, 3 µm, and 1 µm polishing cloths, adjusting the load and time until a scratch-free, mirror-finish surface is achieved. For examining the white layers, the polished samples undergo etching with a 2% nital etchant solution (2 ml nitric acid and 98 ml ethanol) for 7-10 seconds.

### 5.2.4 Optical microscopy

Light optical microscopy (LOM) was employed to visually examine the presence of white layers under varying cutting conditions and tool geometries (paper A-C). Zeiss Axiovision 7 LOM was utilized for this purpose. The use of a Nital etchant resulted in contrasting images that revealed the white and dark layers of the microstructure. A 20x lens was used for an overall observation of continuous or discontinuous white layer formation. Additionally, a 50x magnification allowed for the measurement of white and dark layer thicknesses across different cutting conditions as seen in Figure 10 (a) and (b). However, as the interested features are within 5 µm from the surface, the spatial resolution of this method did not permit a detailed examination of microstructural features, carbide morphology within the white layer, material drag zone, or dark layer.

Stereo optical microscopy (SOM) was employed to capture images of tool wear geometry on cutting inserts, correlating with the resulting surface roughness (Paper B). Zeiss Discovery V20 equipment was utilized for this purpose. Unlike light optical microscopy, stereo optical microscopy had lower magnification and did not require additional preparation of the cutting inserts for observation of tool wear (Figure 10(c)).

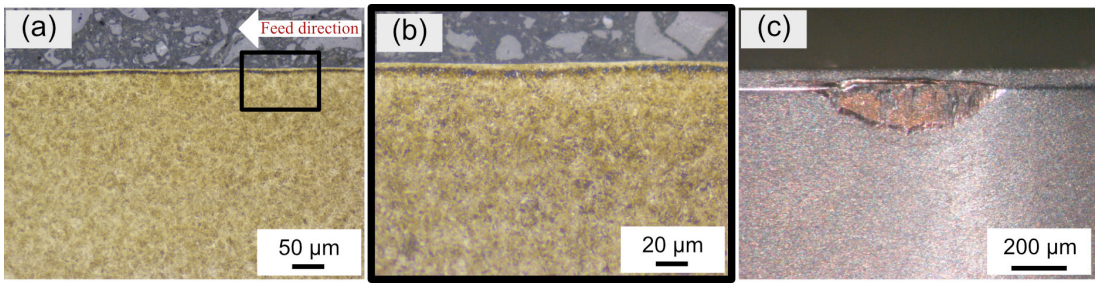


*Figure 10: (a) 20x magnification of the white layer in LOM (b) 50x magnification of the white layer on the machined surface in LOM (c) SOM image of the tool wear on the cutting edge.*

### 5.2.5 Scanning electron microscopy

The scanning electron microscopy (SEM) was performed using a Zeiss Gemini 450 and LEO Gemini 1550 SEM. Secondary electron (SE) imaging mode was used on Nital etched samples by Gemini 450 SEM in this study to observe the white layer microstructure in high magnification mode (Paper A-C). An accelerating voltage of 3 kV and a current of 500 pA with a working distance of 5 mm – 6mm were used. Secondary electron imaging provides insight into the topography of a sample by detecting electrons that escape from its surface. These images result from inelastic interactions between the primary electron beam and the etched sample. Secondary electron imaging employs lower-energy electrons generated from a shallower region within the sample, approximately 10 nm depth, allowing for high-resolution imaging [71]. Figure 11 shows the SE images of the 25% RA content machined sample of different magnifications. The white layer microstructural features are observed due to better spatial resolution in comparison to the LOM.

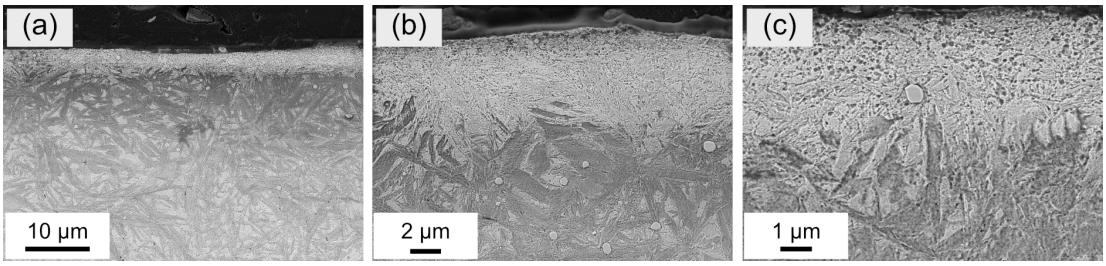


*Figure 11: (a) 5000x magnification SEM image of WL and DL formed on the 25% RA sample (b) 12000x magnification (c) 24000x magnification and carbides are observed in the white layer.*

### 5.2.6 Nanoindentation

The white layers generated on the machined surface are in the range of 1 – 3 µm in thickness. Nanoindentation was performed in both the generated mechanically induced white layer and thermally induced white layer to study the hardness behaviour (Paper B). The measurements were performed using NanoTest Vantage equipment (Micro Materials Ltd.) with a load of 4 mN. The load of 4 mN was selected so that the indentations could be performed within the white layer thickness as seen in Figure 12 below. Hardness was assessed via load and displacement graphs, applying the Oliver-

Pharr method [64]. To accurately measure the hardness values of the white layer without the presence of (Fe, Cr)3C carbides, SEM analysis was conducted on the nanoindentation results.

Nanoindentation is a method employed to assess the mechanical characteristics of small material volumes using a diamond Berkovich indenter. It operates on contact elastic-mechanics theory, wherein the elastic modulus and hardness ($H$) are deduced from the initial unloading curve's slope and the ratio of peak load ($P_{max}$) to contact area ($A_c$), respectively.

$$H = \frac{P_{max}}{A_c} \qquad (5)$$

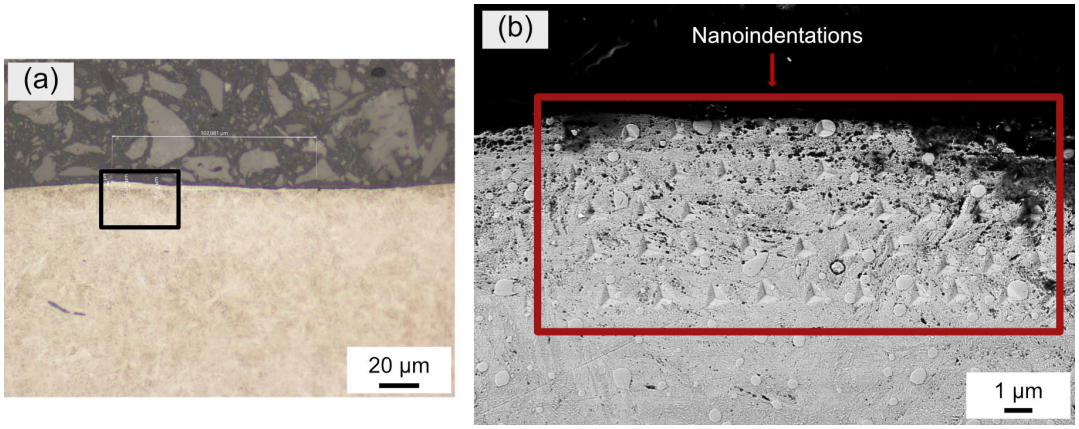


*Figure 12: (a) LOM image of the nanoindentation location (b) SEM image of the nanoindentation performed on the sample.*

# CHAPTER 6

# Summary of Appended Papers

In this chapter, the research questions mentioned in section 1.2 are addressed by summarizing the work from the appended papers. Section 6.1 deals with research question 1 from papers A and B while section 6.2 deals with research question 2 from paper C.

## 6.1 Paper A and Paper B

***Q1: What is the effect of cutting parameters and cutting tool geometry on the surface integrity of the hard-turned AISI 52100 steel?***

Depending on the cutting conditions, the machined surfaces generated by the hard-turning process are subjected to experience different thermo-mechanical loadings resulting in different residual stresses, surface roughness, microstructure, and hardness behavior. From a temperature point of view, the white layers generated on the machined surface can be formed by predominantly thermal influences termed thermally-induced white layer (T-WL) or predominantly mechanical influences termed mechanically-induced white layer (M-WL). The parameters cutting speed ($V_c$), feed rate ($f$), depth of cut ($a_p$), tool chamfer angle ($\gamma$), coolant pressure ($P$), and tool flank wear ($VB$) influence the thermal and mechanical loads resulting in M-WL or T-WL.

The results indicate that machining with a low feed rate of 0.05 mm/rev under all cutting conditions generated a grinding profile rather than the usual hook-shaped profile, as shown by the black curve in Fig. 13 (a). This is due to the uncut chip thickness being smaller than the cutting tool tip radius, resulting in a high compressive state ahead

of the cutting edge. As the feed rate increased, surface compressive stresses decreased due to higher surface temperatures, while deeper sub-surface compressive stresses were observed due to plastic deformation and higher cutting forces. However, with increasing feed rate, surface roughness deteriorated, forming helicoid furrows with increased peak-to-valley distance in feed marks as shown in red colour in Fig. 14. As shown in Figure 6a in paper A, the lowest surface roughness of 0.07 µm is observed with the hard-turning process and is comparable with the roughness obtained by the grinding process.

An increase in chamfer angle led to better surface and sub-surface compressive stresses due to mechanical load effects. Higher cutting speeds of 110 m/min resulted in increased surface cutting temperatures which lower surface compressive stresses. Furthermore, with fresh inserts, the microstructural results showed the generation of discontinuous white layers as shown in Figures 15 (a) and 15 (c). The use of high coolant pressure (150 bar) resulted in better compressive stresses on the surface for low feed rate workpieces. The depth of cut did not significantly affect residual stresses or surface roughness of the machined samples.

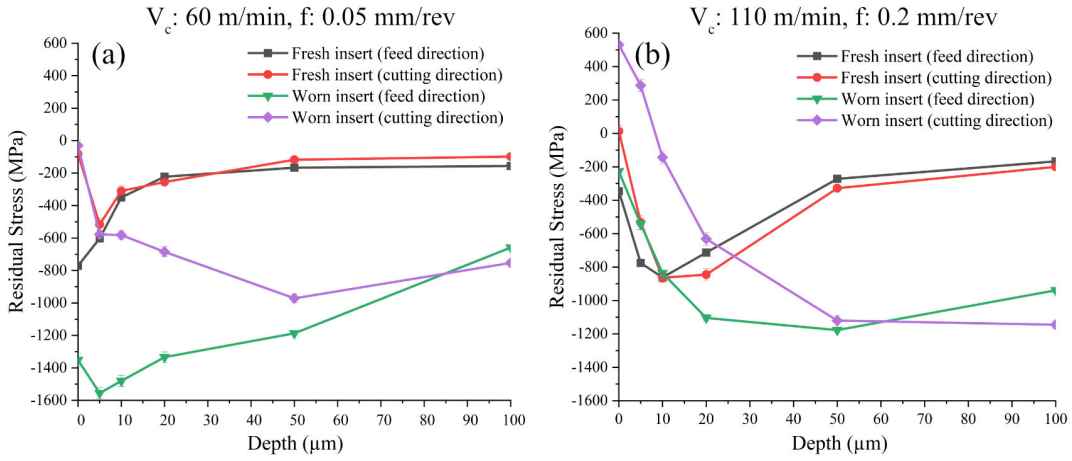


*Figure 13: Residual stress plots for (a) $V_c$: 60 m/min, f: 0.05 mm/rev, (b) $V_c$: 110 m/min, f: 0.2 mm/rev with constant $a_p$: 0.2 mm, γ: 35°, P: 150 bar parameters and the worn insert represents VB: 0.2 mm.*

The effects of cutting speed and feed rate as shown in Figs. 13 and 14 influence the residual stress profiles and surface roughness due to predominantly thermal and mechanical loads. Tool wear further amplifies these effects, generating significantly higher compressive stresses from mechanical effects or resulting in tensile stresses due to high thermal effects. Machining at a low cutting speed of 60 m/min and a low feed rate of 0.05 mm/rev results in higher compressive stresses and reduced surface roughness. In contrast, using a high cutting speed of 110 m/min and a high feed rate of 0.2 mm/rev results in reduced compressive stresses or even tensile stresses along the cutting direction, especially with a worn insert.

Regarding surface roughness, the micro geometry of tool wear causes an increase in surface roughness under both predominantly thermal and mechanical conditions compared to a fresh insert, as shown in Fig. 14. However, the extent of this increase is driven by the cutting speed and feed rate. The predominantly mechanical effect resulted in a roughness of 0.11 µm with the fresh insert and 0.19 µm with the worn insert. In contrast, the predominantly thermal effect resulted in a surface roughness of 0.59 µm with the fresh insert and 1.19 µm with the worn insert. This behaviour indicates the beneficial residual stresses and roughness obtained by the predominantly mechanical effects.

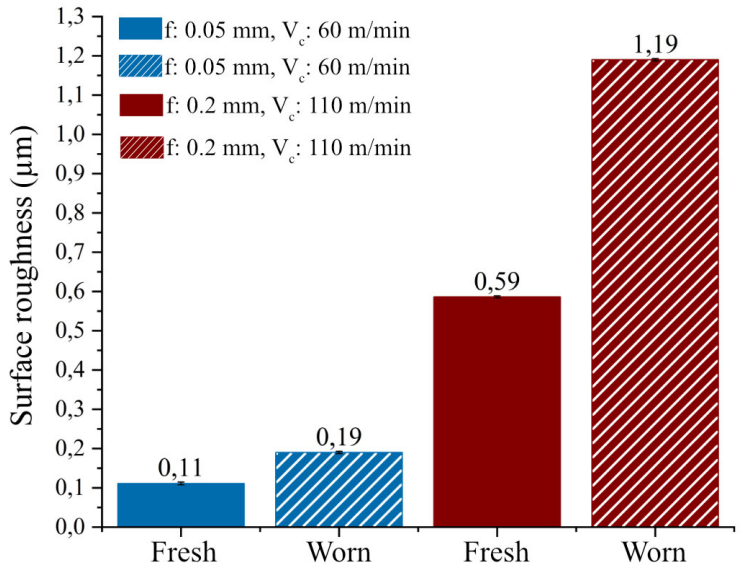


*Figure 14: Surface roughness values for the selected mechanically and thermally influenced parameters (a) $V_c$: 60 m/min, f: 0.05 mm/rev, (b) $V_c$: 110 m/min, f: 0.2 mm/rev with constant $a_p$: 0.2 mm, γ: 35°, P: 150 bar parameters and the worn insert represents VB: ~0.2 mm.*

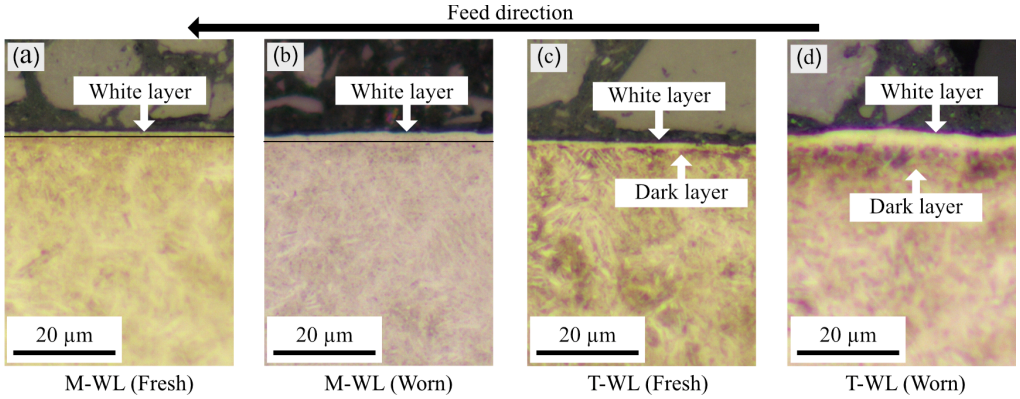


*Figure 15: Optical microscopy (OM) images of the mechanically dominant and thermally dominant machined samples with ap: 0.2 mm, P: 150 bar, γ: 35° constant cutting parameters along the feed direction. (a) Fresh insert, f: 0.05 mm/rev, $V_c$: 60 m/min (M-WL Fresh) (b) VB: ~0.2 mm worn insert, f: 0.05 mm/rev, $V_c$: 60 m/min*

*(M-WL Worn), (c) Fresh insert, f: 0.2 mm/rev, $V_c$: 110 m/min (T-WL Fresh), (d) VB: ~0.2 mm worn insert, f: 0.2 mm/rev, $V_c$: 110 m/min (T-WL Worn).*

Figure 15 shows the OM images of the generated white layer along the feed direction under predominantly mechanical and thermal influences. Low cutting speed of 60 m/min and a low feed rate of 0.05 mm/rev resulted in the formation of a mechanically induced white layer (M-WL) for both fresh and worn inserts. In contrast, a high cutting speed of 110 m/min and a high feed rate of 0.2 mm/rev resulted in the formation of a thermally induced white layer (T-WL) for both fresh and worn inserts. However, in the case of fresh insert, a very thin dark layer was observed compared to the worn insert dark layer for high cutting conditions. This is due to as the flank wear increased, the friction between the tool and workpiece resulted in higher temperatures affecting the subsurface regions generating a thicker dark layer area underneath the white layers.

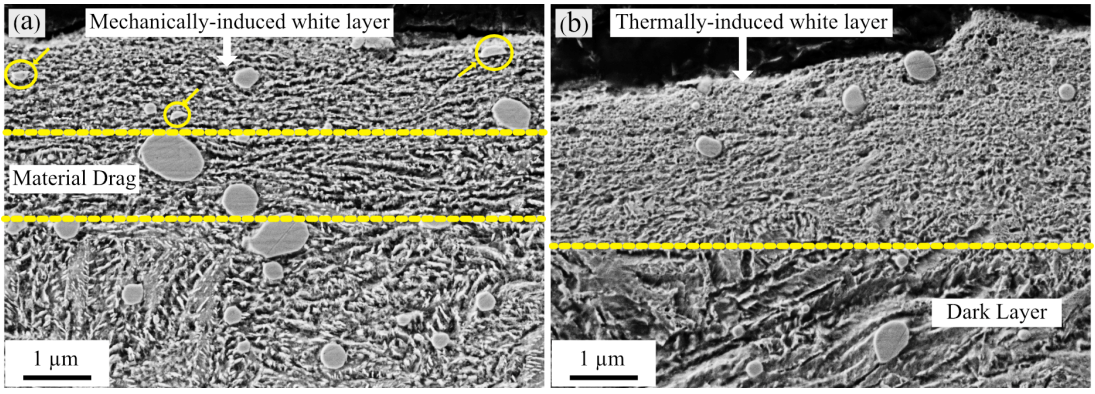


*Figure 16: SEM images of the (a) mechanically-induced white layers (M-WL) accompanied with material drag beneath, and (b) thermally-induced white layers (T-WL) with dark layer generated by worn inserts*

The SEM images reveal that the mechanically induced white layer (M-WL) is formed due to intense plastic deformation, characterized by an elongated and fragmented refined structure along the feed direction and a material drag zone beneath it (see Figure 16 (a)). Figure 16 (b) shows the thermally induced white layer (T-WL) generated under high thermal influence, with a dark layer beneath it. The morphology of M-WL and T-WL is different, indicating distinct formation mechanisms. To further understand the characteristics of M-WL and T-WL, nanoindentation was performed. The nanohardness results for M-WL and T-WL are shown in Figure 17. Both white layers exhibit similar hardness behavior; however, the material drag zone in M-WL has ~6.15% higher hardness than the bulk material, whereas the dark layer in T-WL has a ~17% lower hardness than the bulk. The higher hardness of the M-WL and material drag, along with higher compressive stresses and lower surface roughness, would be beneficial for functional performance compared to T-WL.

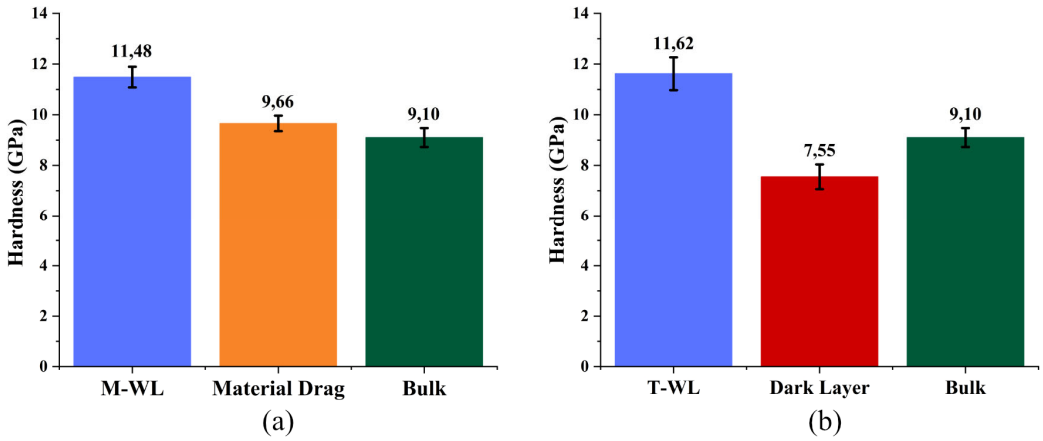


*Figure 17: Nanoindentation results of the (a) Mechanically-induced white layer with material drag beneath, and (b) Thermally-induced white layers with the dark layer beneath*

## 6.2 Paper C

***Q2: What is the role of retained austenite in the formation of hard-turned induced white layers?***

The objective of the research question is to understand the role of retained austenite in the formation of M-WL and T-WL. As shown in Figures 13 and 14 from papers A and B, the M-WL resulted in better surface integrity compared to T-WL and paper C summarizes how the different retained austenite content (<2%, 12%, and 25%) influences the white layer formation.

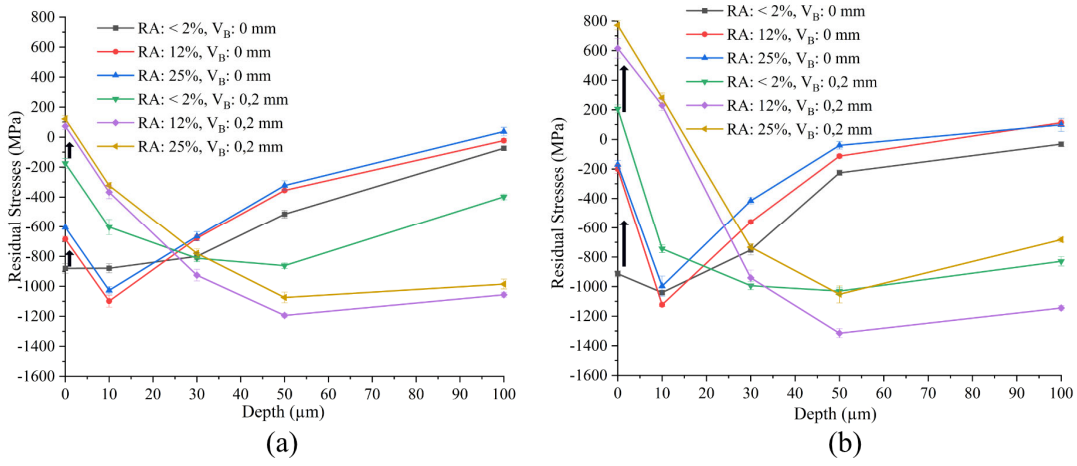


*Figure 18: Residual stresses measured along the cutting direction for different retained austenite fractions and tool wear with cutting speed of (a) $V_c$: 60m/min and (b) $V_c$: 260m/min.*

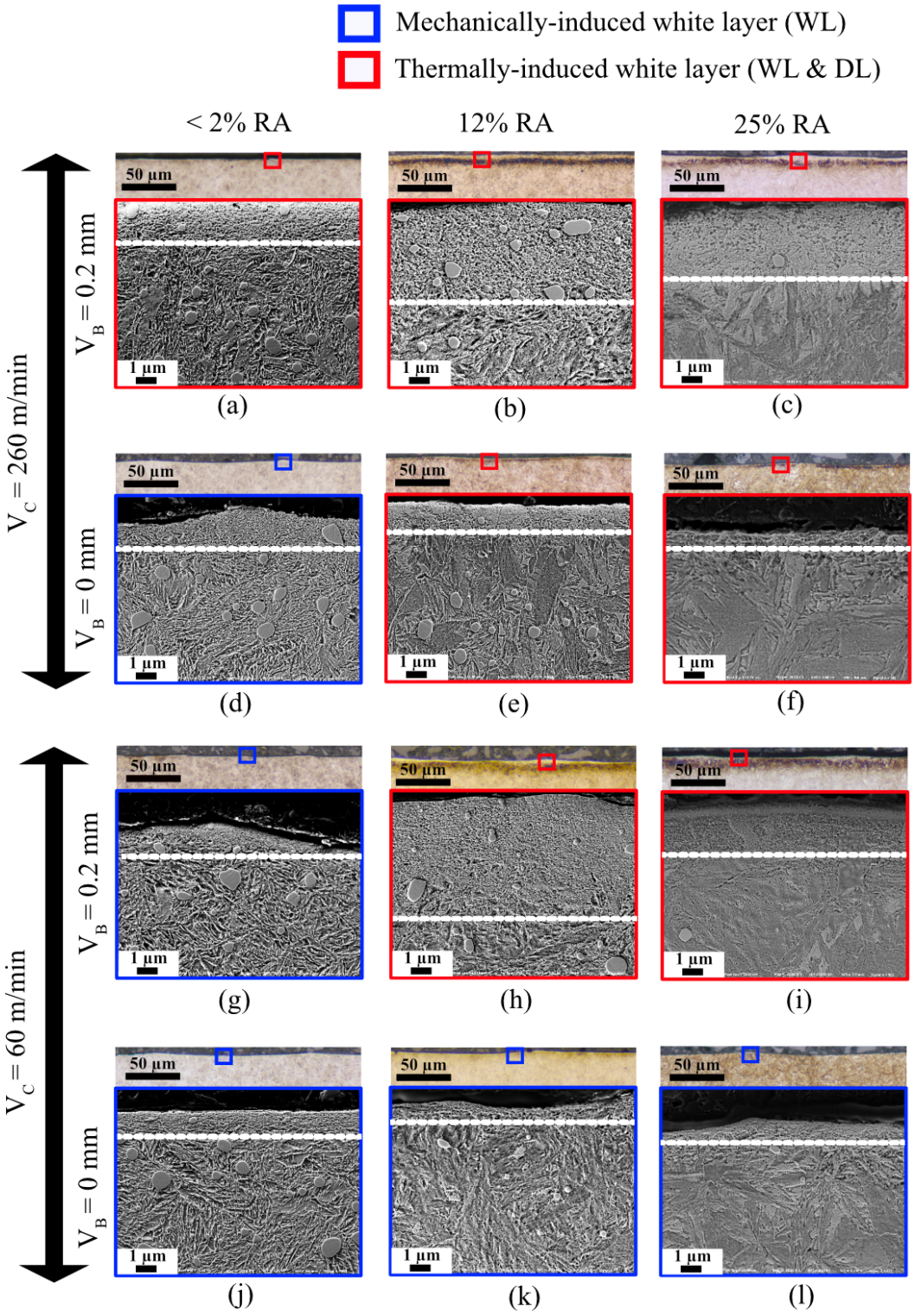


*Figure 19: Light optical microscopy (LOM) and their respective scanning electron microscopy images of samples machined with different cutting conditions. The white dashed lines indicate the boundary between the white layer and the bulk for the mechanically-induced white layer and the boundary between the white layer and dark layer for the thermally-induced white layer.*

Figure 18 shows the residual stress profiles along the cutting direction for different retained austenite content and tool wear with (a) $V_c$: 60m/min and (b) $V_c$: 260m/min. In both cutting speed conditions, the higher retained austenite contents (12% and 25%) resulted in reduced surface compressive stresses with a fresh insert and generated tensile stresses with a worn insert. The increased cutting speed of 260 m/min resulted in much higher tensile stresses of 600 – 800 MPa with worn inserts due to an increase in surface temperature. Samples with <2% retained austenite content observed surface tensile stresses of 200 MPa at 260 m/min with a worn insert.

Further to understand the increase in surface tensile residual stresses for worn insert and lower surface compressive stresses for fresh insert in 12% and 25% RA content samples compared to <2% RA content, microstructural study was performed. The corresponding microstructures shown in Fig. 19 relate well to the observed residual stress profiles. The higher tensile stresses resulted in the formation of thermally-induced white layers for 12% and 25% RA content samples. When all the samples observed higher surface compressive stresses, this is due to the formation of mechanically induced white layers for 60 m/min and fresh insert conditions.

Higher RA content promotes the formation of a thermally induced white layer with increased tool wear and cutting speed. Even though the T-WL is observed for <2% RA content at 260 m/min with a worn tool, the thickness of the generated T-WL is very thin as shown in Fig. 19 (a) compared to Fig. 19 (b) and (c). The influence of specific cutting pressure on the austenitization temperature is significant. The austenite phase (FCC) being denser than tempered martensite (BCC) concerning the atomic packing fraction will reduce the austenitization temperature due to the cutting pressure effect. Also, the low stacking fault energy of austenite inhibits dynamic recovery and promotes dynamic recrystallization resulting in the formation of T-WL. However, to fully understand the underlying mechanisms of how the retained austenite affects the WL formation, and its final characteristics, a detailed investigation of the austenitization temperature is necessary. In such work, the influence of heating rate, strain, pressure, and carbon concentration must be included.

# CHAPTER 7

# Conclusions and Future Work

## 7.1 Conclusions

Q1: What is the effect of cutting parameters and cutting tool geometry on the surface integrity of the hard-turned AISI 52100 steel?

- The samples machined with low $V_c$: 60 m/min, low f: 0.05 mm/rev with constant $a_p$: 0.2 mm, P: 150 bar, and γ: 35° conditions resulted in better surface roughness and higher surface compressive stresses with mechanically induced white layers (M-WL) on the machined surface.
- The samples machined with high $V_c$: 110 m/min, high f: 0.2 mm/rev with constant $a_p$: 0.2 mm, P: 150 bar, and γ: 35° conditions showed increased surface roughness and reduced surface compressive stresses with fresh inserts, and surface tensile stresses with worn inserts, forming thermally induced white layers (T-WL) on the machined surface.
- The white layer morphology for M-WL and T-WL appears different when observed by SEM.
- The M-WL exhibited an elongated and fragmented microstructure with hardness 26% higher than the bulk material, while the material drag zone observed beneath had a 6.15% higher hardness than the bulk material.
- The T-WL exhibited 27.6% higher hardness than the bulk material, while the dark layer beneath had 17% lower hardness than the bulk material.

Q2: What is the role of retained austenite in the formation of hard-turned induced white layers?

- Regardless of RA content, a low cutting speed of 60 m/min using fresh cutting inserts, resulted in M-WLs accompanied by surface compressive residual stresses.
- For samples with 12% and 25% RA and when the tool flank wear increased to 0.2 mm while machining at 60 m/min, the formation of T-WL was observed which was accompanied by surface tensile residual stresses. A similar observation was made when machining at 260 m/min using a fresh cutting insert.
- Regardless of RA content, all surfaces were characterized by T-WL that were accompanied by surface tensile residual stresses when machined at 260 m/min with a worn cutting tool (VB: 0.2 mm).

## 7.2 Future work

In the thesis, the cutting parameters leading to mechanically induced and thermally induced white layers are investigated. However, to understand the functional performances of the generated white layers, the following investigations are recommended for future work:

- To investigate the wear mechanism and fatigue performances of M-WL and T-WL surfaces and compare them with ground specimens.
- To perform transmission electron microscopy and atom probe tomography to study the differences in white layers (M-WL /T-WL) generated using fresh and worn inserts and the adjacent material drag and dark layer microstructures.
- To perform the EBSD analysis using transmission kikuchi diffraction to study the orientation mapping for the M-WL and T-WL.
- Further, to investigate the role of high retained austenite content in reducing the austenitization temperature.

# Acknowledgements

I would like to express my deepest gratitude to my supervisors, Prof. Uta Klement and Dr. Seyed B Hosseini, for providing me with this exceptional opportunity and for their unwavering guidance in scientific research and career development during this journey. Additionally, I would like to thank my examiner Prof. Peter Krajnik for his support during this time.

I extend my thanks to the Turn2Flex project members who supported me with their valuable input throughout this time. A special thanks to Dr. Jonas Holmberg from RISE IVF AB for his guidance with residual stresses, surface roughness measurements, and project discussions. I would like to thank Wolfgang Neuhs and Hirotsugu Iwasaki from Sumitomo Electric Hardmetal Corp. for their support with hard-turning experiments. I would like to thank Stefan Kimming and Roger Lundstrom from SKF AB for their support in preparing the worn inserts and performing hard-turning experiments. My thanks also go to Dr. Bjork Thomas from Ovako for his support with the samples and valuable insights. I would like to thank Thord Johansson from SST for his valuable suggestions and encouragement. I would also like to thank Ulrika Elmersson and Martina Elf from SKTC for their support in this project and for ensuring the gained knowledge can be transferred to small and medium enterprises.

I would like to thank Adrian Harris and Gerard Irwin from Micro Materials Ltd. for their support with the nanoindentation measurements in a short time.

Furthermore, I would like to thank the research engineers Dr. Yiming Yao, Dr. Antonio Mulone, and Dr. Eric Tam. I would like to acknowledge the support from administrative staff Jessica Twedmark for her help with the onboarding.

Thanks to my friends and colleagues at the department for their support and for making my life happier at Chalmers. I would like to especially thank Bala and Anok for their guidance and support throughout my time in Sweden. I am very grateful to Vishnu, Daniel, Erika, Plinio, Fardan and many others including the volleyball team for all the fun and good times outside work.

To my dear friends, Reddy, Kalyan, Vardan, Vishnu, Diwakar, Srikanth, Nithin and a few more I met in the Netherlands and the boys back from my hometown Ramagundam, thank you for being there for me.

I can’t thank my parents enough for their unwavering support and for standing by my side all these years and would like to send my deepest gratitude to them for understanding me. I am very much grateful to my brother Rohith for choosing Sweden for his master's and being closer to me. I am also grateful to my family, especially Meghana and Bhavana for being with me and supporting me always. Lastly, I would like to thank my girlfriend Sophia for all her love and support during this interesting journey.

Sahith Kokkirala
May, 2024

# References


[1] H. K. Tönshoff, C. Ardent, and R. Ben Amor, “Cutting of Hardened Steel,” *CIRP Ann Manuf Technol*, vol. 49, no. 2, pp. 1–19, 2000.

[2] N. Jouini, P. Revel, and G. Thoquenne, “Influence of surface integrity on fatigue life of bearing rings finished by precision hard turning and grinding,” *J Manuf Process*, vol. 57, no. February, pp. 444–451, 2020, doi: 10.1016/j.jmapro.2020.07.006.

[3] S. Chinchanikar and S. K. Choudhury, “Machining of hardened steel - Experimental investigations, performance modeling and cooling techniques: A review,” *Int J Mach Tools Manuf*, vol. 89, pp. 95–109, 2015, [Online]. Available: http://dx.doi.org/10.1016/j.ijmachtools.2014.11.002

[4] B. J. Griffiths, “White layer formations at machined surfaces and their relationship to white layer formatins at worn surfaces.,” vol. 107, no. April, pp. 165–171, 1984.

[5] A. A. Torrance, “The metallography of worn surfaces and some theories of wear,” *Wear*, vol. 56, no. 2, pp. 424–426, 1979, doi: 10.1016/0043-1648(79)90246-1.

[6] I. P. Kruth, I. Stevens, I. Froyen, and I. Lauwers, “Study of the White Layer of a Surface Machined by Die-Sinking Electro-Discharge Machining,” *CIRP Ann Manuf Technol*, vol. 44, no. 1, pp. 169–172, 1995, doi: 10.1016/S0007-8506(07)62299-9.

[7] M. C. Shaw and A. Vyas, “Heat-Affected Zones in Grinding Steel,” *CIRP Ann Manuf Technol*, vol. 43, no. 1, pp. 279–282, 1994, doi: 10.1016/S0007-8506(07)62213-6.

[8] J. Barry and G. Byrne, “TEM study on the surface white layer in two turned hardened steels,” *Materials Science and Engineering: A*, vol. 325, no. 1–2. pp. 356–364, 2002.

[9] S. B. Hosseini, U. Klement, Y. Yao, and K. Ryttberg, “Formation mechanisms of white layers induced by hard turning of AISI 52100 steel,” *Acta Mater*, vol. 89, pp. 258–267, 2015, [Online]. Available: http://dx.doi.org/10.1016/j.actamat.2015.01.075

[10] R. Hossain *et al.*, “Hybrid structure of white layer in high carbon steel - Formation mechanism and its properties,” *Sci Rep*, vol. 7, no. 1, pp. 1–12, 2017, doi: 10.1038/s41598-017-13749-7.

[11] J. Stead, “Micro-metallography and its practical applications,” *Journal of Western Scottish Iron and Steel Institute*, vol. 19, pp. 169–204, 1912.

[12] A. M. Wusatowska-Sarnek, B. Dubiel, A. Czyrska-Filemonowicz, P. R. Bhowal, N. Ben Salah, and J. E. Klemberg-Sapieha, “Microstructural characterization of the white etching layer in nickel-based superalloy,” *Metall Mater Trans A Phys Metall Mater Sci*, vol. 42, no. 12, pp. 3813–3825, 2011, doi: 10.1007/s11661-011-0779-8.

[13] J. G. Li, M. Umemoto, Y. Todaka, and K. Tsuchiya, “Nanocrystalline structure formation in carbon steel introduced by high speed drilling,” *Materials Science and Engineering: A*, vol. 435–436, pp. 383–388, 2006, doi: 10.1016/j.msea.2006.07.036.

[14] D. M. Turley, “The nature of the white-etching surface layers produced during reaming ultra-high strength steel,” *Materials Science and Engineering*, vol. 19, no. 1, pp. 79–86, 1975, doi: 10.1016/0025-5416(75)90010-5.

[15] S. B. Hosseini, U. Klement, and J. Kaminski, “Microstructure characterization of white layer formed by hard turning and wire electric discharge machining in high carbon steel (AISI 52100),” *Adv Mat Res*, vol. 409, no. i, pp. 684–689, 2012, doi: 10.4028/www.scientific.net/AMR.409.684.

[16] A. Kumar, G. Agarwal, R. Petrov, S. Goto, J. Sietsma, and M. Herbig, “Microstructural evolution of white and brown etching layers in pearlitic rail steels,” *Acta Mater*, vol. 171, pp. 48–64, 2019, doi: 10.1016/j.actamat.2019.04.012.

[17] Y. K. Chou and C. J. Evans, “White Layers and Thermal Modeling of Hard Turned Surfaces,” *ASME International Mechanical Engineering Congress and Exposition, Proceedings (IMECE)*, vol. 1997-W, pp. 75–82, 1997, doi: 10.1115/IMECE1997-1138.

[18] Y. B. Guo and J. Sahni, “A comparative study of hard turned and cylindrically ground white layers,” *Int J Mach Tools Manuf*, vol. 44, no. 2–3, pp. 135–145, 2004, doi: 10.1016/j.ijmachtools.2003.10.009.

[19] J. A. Bailey, S. Jeelani, and S. E. Becker, “Surface Integrity in Machining AiSI 4340 Steel,” *J. Eng. Ind. (Trans. ASME)*, vol. 98, no. 3, pp. 999–1007, 1976.

[20] S. Han, S. N. Melkote, M. S. Haluska, and T. R. Watkins, “White layer formation due to phase transformation in orthogonal machining of AISI 1045 annealed steel,” *Materials Science and Engineering: A*, vol. 488, no. 1–2, pp. 195–204, 2008, doi: 10.1016/j.msea.2007.11.081.

[21] F. yuan Zhang, C. zheng Duan, M. jie Wang, and W. Sun, “White and dark layer formation mechanism in hard cutting of AISI52100 steel,” *J Manuf Process*, vol. 32, no. March, pp. 878–887, 2018, doi: 10.1016/j.jmapro.2018.04.011.

[22] A. Ramesh, S. N. Melkote, L. F. Allard, L. Riester, and T. R. Watkins, “Analysis of white layers formed in hard turning of AISI 52100 steel,” *Materials Science and Engineering: A*, vol. 390, no. 1–2, pp. 88–97, 2005.

[23] S. Akcan, W. I. S. Shah, S. P. Moylan, P. N. Chhabra, S. Chandrasekar, and H. T. Y. Yang, “Formation of white layers in steels by machining and their characteristics,” *Metall Mater Trans A Phys Metall Mater Sci*, vol. 33, no. 4, pp. 1245–1254, 2002.

[24] V. Bedekar, R. Shivpuri, R. Chaudhari, and R. S. Hyde, “Nanostructural evolution of hard turning layers in response to insert geometry, cutting parameters and material microstructure,” *CIRP Ann Manuf Technol*, vol. 62, no. 1, pp. 63–66, 2013.

[25] S. B. Hosseini and U. Klement, “A descriptive phenomenological model for white layer formation in hard turning of AISI 52100 bearing steel,” *CIRP J Manuf Sci Technol*, vol. 32, pp. 299–310, 2021, [Online]. Available: https://doi.org/10.1016/j.cirpj.2021.01.014

[26] S. P. F. C. Jaspers and J. H. Dautzenberg, “Material behaviour in metal cutting: Strains, strain rates and temperatures in chip formation,” *J Mater Process Technol*, vol. 121, no. 1, pp. 123–135, 2002, doi: 10.1016/S0924-0136(01)01227-4.

[27] G. Poulachon, A. Moisan, and I. S. Jawahir, “On modelling the influence of thermo-mechanical behavior in chip formation during hard turning of 100Cr6 bearing steel,” *CIRP Ann Manuf Technol*, vol. 50, no. 1, pp. 31–36, 2001, doi: 10.1016/S0007-8506(07)62064-2.

[28] C. Zener and J. H. Hollomon, “Effect of strain rate upon plastic flow of steel,” *J Appl Phys*, vol. 15, no. 1, pp. 22–32, 1944, doi: 10.1063/1.1707363.

[29] U. Takashi, H. Mahfudz Al, Y. Keiji, and N. Kazuo, “Temperature Measurement of CBN Tool in Turning of High Hardness Steel,” *Annals of the CIRP*, vol. 48, no. 1, pp. 63–66, 1999.

[30] S. B. Hosseini, T. Beno, U. Klement, J. Kaminski, and K. Ryttberg, “Cutting temperatures during hard turning—Measurements and effects on white layer formation in AISI 52100,” *J Mater Process Technol*, vol. 214, no. 6, pp. 1293–1300, Jun. 2014, [Online]. Available: https://linkinghub.elsevier.com/retrieve/pii/S0924013614000399

[31] B. Zhang, W. Shen, Y. Liu, X. Tang, and Y. Wang, “Microstructures of surface white layer and internal white adiabatic shear band,” *Wear*, vol. 211, no. 2, pp. 164–168, 1997, doi: 10.1016/S0043-1648(97)00099-9.

[32] M. Sun, L. Hao, S. Li, D. Li, and Y. Li, “Modeling flow stress constitutive behavior of SA508-3 steel for nuclear reactor pressure vessels,” *Journal of Nuclear Materials*, vol. 418, no. 1–3, pp. 269–280, 2011, doi: 10.1016/j.jnucmat.2011.07.011.

[33] H. J. McQueen and C. A. C. Imbert, “Dynamic recrystallization: Plasticity enhancing structural development,” *J Alloys Compd*, vol. 378, no. 1–2, pp. 35–43, 2004, doi: 10.1016/j.jallcom.2003.10.067.

[34] C. Z. Duan and L. C. Zhang, “Adiabatic shear banding in AISI 1045 steel during high speed machining: Mechanisms of microstructural evolution,” *Materials Science and Engineering: A*, vol. 532, pp. 111–119, 2012, doi: 10.1016/j.msea.2011.10.071.

[35] H. J. McQueen, “The production and utility of recovered dislocation substructures,” *Metallurgical Transactions A*, vol. 8, no. 6, pp. 807–824, 1977, doi: 10.1007/BF02661562.

[36] H. Q. Sun, Y. N. Shi, M. X. Zhang, and K. Lu, “Plastic strain-induced grain refinement in the nanometer scale in a Mg alloy,” *Acta Mater*, vol. 55, no. 3, pp. 975–982, 2007, doi: 10.1016/j.actamat.2006.09.018.

[37] W. Li, T. Sakai, Q. Li, L. T. Lu, and P. Wang, “Reliability evaluation on very high cycle fatigue property of GCr15 bearing steel,” *Int J Fatigue*, vol. 32, no. 7, pp. 1096–1107, 2010, doi: 10.1016/j.ijfatigue.2009.12.008.

[38] A. M. Cree, R. G. Faulkner, and A. T. Lyne, “Cementite particle coarsening during spheroidisation of bearing steel SAE 52100,” *Materials Science and Technology (United Kingdom)*, vol. 11, no. 6, pp. 566–571, 1995, doi: 10.1179/mst.1995.11.6.566.

[39] A. T. W. Barrow and P. E. J. Rivera-Díaz-Del-Castillo, “Nanoprecipitation in bearing steels,” *Acta Mater*, vol. 59, no. 19, pp. 7155–7167, 2011, doi: 10.1016/j.actamat.2011.08.007.

[40] H. K. D. H. Bhadeshia, “Steels for bearings,” *Prog Mater Sci*, vol. 57, no. 2, pp. 268–435, 2012, doi: 10.1016/j.pmatsci.2011.06.002.

[41] M. Perez, C. Sidoroff, A. Vincent, and C. Esnouf, “Microstructural evolution of martensitic 100Cr6 bearing steel during tempering: From thermoelectric power measurements to the prediction of dimensional changes,” *Acta Mater*, vol. 57, no. 11, pp. 3170–3181, 2009, doi: 10.1016/j.actamat.2009.03.024.

[42] K. Cao, Z. Wang, P. Liu, and A. Zhao, “Effect of austenitizing temperature and cooling rate on Ms temperature of Fe–Ni–Cr cast iron,” *Journal of Materials Research and Technology*, vol. 26, pp. 796–806, 2023, doi: 10.1016/j.jmrt.2023.07.208.

[43] L. D. Barlow and M. Du Toit, “Effect of austenitizing heat treatment on the microstructure and hardness of martensitic stainless steel AISI 420,” *J Mater Eng Perform*, vol. 21, no. 7, pp. 1327–1336, 2012, doi: 10.1007/s11665-011-0043-9.

[44] C. S. Smith, “A History of Metallography: The Development of Ideas on the Structure of Metals Before 1890.,” *The MIT. Press*, 1988.

[45] H. Bhadeshia and R. Honeycombe, *Formation of Martensite*, 4th ed. Elsevier Ltd, 2017. doi: 10.1016/b978-0-08-100270-4.00005-6.

[46] C. S. Roberts, “Effect of Carbon on the Volume Fractions and Lattice Parameters Of Retained Austenite and Martensite,” *Jom*, vol. 5, no. 2, pp. 203–204, 1953, doi: 10.1007/bf03397477.

[47] G. Krauss, *Tempering of martensite in carbon steels*. Woodhead Publishing Limited, 2012. doi: 10.1533/9780857096111.1.126.

[48] F. Klocke and A. Kuchle, *Manufacturing Process 1*. 2001.

[49] L. N. López De Lacalle, A. Lamikiz, J. Fernández De Larrinoa, and I. Azkona, “Advanced cutting tools,” *Machining of Hard Materials*, pp. 33–86, 2011, doi: 10.1007/978-1-84996-450-0_2.

[50] J.-E. Ståhl and S. T. AB, *Metal Cutting: Theories and Models*. Division of Production and Materials Engineering, 2012.

[51] W. Grzesik, “Cutting Tool Materials,” in *Advanced Machining Processes of Metallic Materials*, 2nd Editio., W. Grzesik, Ed., Elsevier B.V., 2017, pp. 35–63.

[52] W. Grzesik, “Tool Wear and Damage,” in *Advanced Machining Processes of Metallic Materials*, Elsevier B.V., 2017, pp. 215–239.

[53] W. Grzesik, “Advanced Machining Processes,” in *Advanced Machining Processes of Metallic Materials*, Elsevier B.V., 2017, pp. 285–397.

[54] M. Field and J. F. Kahles, “Review of surface integrity of machined components,” *CIRP Annals*, vol. 20, no. 2, pp. 153–163, 1971.

[55] W. Grzesik, “Surface Integrity,” in *Advanced Machining Processes of Metallic Materials*, Elsevier B.V., 2017, pp. 533–561.

[56] A. M. Abrão, J. L. S. Ribeiro, and J. P. Davim, “Surface Integrity,” in *Machining of Hard Materials*, 2011, pp. 115–141. [Online]. Available: https://doi.org/10.1007/978-1-84996-450-0_4

[57] P. J. Withers and H. K. D. H. Bhadeshia, “Residual stress part 2 - Nature and origins,” *Materials Science and Technology*, vol. 17, no. 4, pp. 366–375, 2001, doi: 10.1179/026708301101510087.

[58] V. G. Navas, O. Gonzalo, and I. Bengoetxea, “Effect of cutting parameters in the surface residual stresses generated by turning in AISI 4340 steel,” *Int J Mach Tools Manuf*, vol. 61, pp. 48–57, 2012, doi: 10.1016/j.ijmachtools.2012.05.008.

[59] P. Dahlman, F. Gunnber, and M. Jacobson, “The influence of rake angle, cutting feed and cutting depth on residual stresses in hard turning,” *J Mater Process Technol*, vol. 147, pp. 181–184, 2004, doi: 10.1016/j.matprotec.2003.12.014.

[60] F. Gunnberg, M. Escursell, and M. Jacobson, “The influence of cutting parameters on residual stresses and surface topography during hard turning of 18MnCr5 case carburised steel,” *J Mater Process Technol*, vol. 174, no. 1–3, pp. 82–90, 2006, doi: 10.1016/j.jmatprotec.2005.02.262.

[61] S. Kokkirala, J. Holmberg, U. Klement, R. Lundstrom, H. Iwasaki, and S. B. Hosseini, “Effect of cutting parameters on the generated surface integrity of hard-turned martensitic AISI 52100 bearing steel,” *Procedia CIRP*, vol. 115, pp. 154–159, 2022, doi: 10.1016/j.procir.2022.10.066.

[62] J. Hua *et al.*, “Effect of feed rate, workpiece hardness and cutting edge on subsurface residual stress in the hard turning of bearing steel using chamfer + hone cutting edge geometry,” *Materials Science and Engineering: A*, vol. 394, no. 1–2, pp. 238–248, 2005, doi: 10.1016/j.msea.2004.11.011.

[63] Y. Matsumoto, F. Hashimoto, and G. Lahoti, “Surface integrity generated by precision hard turning,” *CIRP Ann Manuf Technol*, vol. 48, no. 1, pp. 59–62, 1999, doi: 10.1016/S0007-8506(07)63131-X.

[64] A. M. Abrão and D. K. Aspinwall, “The surface integrity of turned and ground hardened bearing steel,” *Wear*, vol. 196, no. 1–2, pp. 279–284, 1996, doi: 10.1016/0043-1648(96)06927-X.

[65] M. Liu, J. I. Takagi, and A. Tsukuda, “Effect of tool nose radius and tool wear on residual stress distribution in hard turning of bearing steel,” *J Mater Process Technol*, vol. 150, no. 3, pp. 234–241, 2004, doi: 10.1016/j.jmatprotec.2004.02.038.

[66] W. König, A. Berktold, and K. F. Koch, “Turning versus Grinding - A Comparison of Surface Integrity Aspects and Attainable Accuracies,” *CIRP Ann Manuf Technol*, vol. 42, no. 1, pp. 39–43, 1993, doi: 10.1016/S0007-8506(07)62387-7.

[67] P. I. Varela, C. S. Rakurty, and A. K. Balaji, “Surface integrity in hard machining of 300M Steel: Effect of cutting-edge geometry on machining induced residual stresses,” *Procedia CIRP*, vol. 13, pp. 288–293, 2014, doi: 10.1016/j.procir.2014.04.049.

[68] G. C. Benga and A. M. Abrao, “Turning of hardened 100Cr6 bearing steel with ceramic and PCBN cutting tools,” vol. 144, pp. 237–241, 2003, doi: 10.1016/S0924-0136(03)00346-7.

[69] J. D. Thiele and S. N. Melkote, “Effect of cutting edge geometry and workpiece hardness on surface generation in the finish hard turning of AISI 52100 steel,” *J Mater Process Technol*, vol. 94, no. 2, pp. 216–226, 1999, doi: 10.1016/S0924-0136(99)00111-9.

[70] H. A. Kishawy and M. A. Elbestawi, “Effects of process parameters on material side flow during hard turning,” *Int J Mach Tools Manuf*, vol. 39, no. 7, pp. 1017–1030, 1999, doi: 10.1016/S0890-6955(98)00084-4.

[71] L. Reimer, *Scanning Electron Microscopy: Physics of Image Formation and Microanalysis, Second Edition*, vol. 11, no. 12. Springer, 2000. doi: 10.1088/0957-0233/11/12/703.